Full paper

New insights into the mechanisms of post-rubisco isotope fractionation from combined analysis of intramolecular ^{13}C and deuterium abundances in *Pinus nigra* tree-ring glucose

Thomas Wieloch[1,2,*], Meisha Holloway-Phillips[3], Jun Yu[4], Totte Niittylä[1]

[1] Department of Forest Genetics and Plant Physiology, Swedish University of Agricultural Sciences, Umeå Plant Science Centre, 90183 Umeå, Sweden

[2] Division of Geological and Planetary Sciences, California Institute of Technology, 91125 Pasadena, USA

[3] Research Unit of Forest Dynamics, Swiss Federal Institute for Forest, Snow and Landscape Research WSL, 8903 Birmendsorf, Switzerland

[4] Department of Mathematics and Mathematical Statistics, Umeå University, 90187 Umeå, Sweden

* Corresponding author, Thomas Wieloch, thomas.wieloch@slu.se

Keywords: carbon stable isotopes, hydrogen stable isotopes, intramolecular isotope analysis, isotope fractionation mechanisms, leaf water status, plant-environment interactions, stem water status, tree rings

6492 words (Introduction, Material and Methods, Results, Discussion), 5 Figures (colour), 7 Tables, Supporting Information including 3 Notes, 6 Tables, and 1 Figure

Author	Email address	ORCID
Thomas Wieloch	thomas.wieloch@slu.se	0000-0001-9162-2291
Meisha Holloway-Phillips	meisha.holloway@wsl.ch	0000-0002-8353-3536
Jun Yu	jun.yu@umu.se	0000-0001-5673-620X
Totte Niittylä	totte.niittyla@slu.se	0000-0001-8029-1503

Summary

Understanding isotope fractionation mechanisms is fundamental for analyses of plant ecophysiology and paleoclimate based on tree-ring isotope data.

To provide new insights into isotope fractionation, we analysed intramolecular ^{13}C discrimination in tree-ring glucose (Δ_i', i = C-1 to C-6) and metabolic deuterium fractionation at H^1 and H^2 (ε_{met}) combinedly.

This dual-isotope approach enabled deconvolution of isotope signals. We found evidence for physiological processes affecting Δ_1' and Δ_3' which respond to air vapour pressure deficit (*VPD*), and processes affecting Δ_1', Δ_2', and ε_{met} which respond to precipitation but not *VPD*. These relationships exhibit change points dividing a period of homeostasis (1961-1980) from a period of metabolic adjustment (1983-1995). Homeostasis may result from sufficient groundwater availability. Additionally, we found Δ_5' and Δ_6' relationships with radiation and temperature which are temporally stable and consistent with previously proposed isotope fractionation mechanisms.

Based on the multitude of climate covariables, intramolecular carbon isotope analysis has an extraordinary potential for climate reconstruction. While isotope fractionation beyond leaves is usually considered to be constant, we propose significant parts of the carbon and hydrogen isotope variation in tree-ring glucose originate in stems (precipitation-dependent signals). As basis for follow-up studies, we propose mechanisms introducing Δ_1', Δ_2', Δ_3', and ε_{met} variability.

Introduction

Analysis of the systematic $^{13}C/^{12}C$ variation (commonly termed "^{13}C signal"; abbreviations in Table 1) across tree-ring series is widely used to study physiological traits such as water-use efficiency, plant-environment interactions, and past climate conditions (Leavitt & Roden, 2022). Signals found at the whole-tissue or whole-molecule level (Fig. 1A, top and middle) are commonly interpreted based on a simple mechanistic model of ^{13}C discrimination, Δ (denoting $^{13}C/^{12}C$ variation caused by physiological processes) (Farquhar *et al.*, 1982). This model considers isotope effects of CO_2 diffusion from ambient air into intercellular air spaces (Craig, 1953) and CO_2 assimilation by rubisco (Roeske & O'Leary, 1984) and phospho*enol*pyruvate carboxylase (PEPC; Fig. 2) (Farquhar, 1983; Farquhar & Richards, 1984). Manifestation of these effects as ^{13}C discrimination depends on the ratio of intercellular-to-ambient CO_2 partial pressure (p_i/p_a) (Farquhar *et al.*, 1982), and a highly significant relationship between p_i/p_a and leaf Δ was confirmed experimentally (Evans *et al.*, 1986). Environmental parameters influence p_i/p_a and thus leaf Δ (Evans *et al.*, 1986) by affecting stomatal regulation and CO_2 assimilation. For instance, in response to drought, isohydric plant species such as *Pinus nigra* (studied here) close their stomata (McDowell *et al.*, 2008). This can be expected to decrease p_i/p_a and leaf Δ (Farquhar *et al.*, 1982; Evans *et al.*, 1986).

Isotope fractionation in downstream metabolism is complex (Hobbie & Werner, 2004), incompletely understood (Badeck *et al.*, 2005; Cernusak *et al.*, 2009) and has yet to be adequately integrated into ^{13}C-discrimination models (Ubierna *et al.*, 2022). Specifically, the simple ^{13}C discrimination model requires multiple adaptations to enable correct interpretation of the ^{13}C composition of tree-ring glucose (studied here). For instance, we recently argued that incorporation of carbon assimilated by PEPC into tree-ring glucose is negligible due to negligible gluconeogenesis in leaves (Fig. 2) (Wieloch *et al.*, 2022c). Therefore, all carbon in tree-ring glucose proposedly derives from rubisco-assimilated CO_2. Since rubisco catalyses a single-carbon addition to ribulose 1,5-bisphosphate (RuBP), ^{13}C discrimination accompanying CO_2 diffusion and rubisco assimilation should affect all glucose carbon positions equally (Wieloch *et al.*, 2018, 2022c).

Furthermore, we recently measured Δ intramolecularly at all six carbon positions, *i*, of glucose (Fig. 1A, bottom) extracted across an annually resolved tree-ring series of *Pinus nigra* (Wieloch *et al.*, 2018). The resultant Δ_i' dataset comprises 6*31 values (study period: 1961 to 1995; four years missing: 1977, 1978, 1981, 1982) which were corrected for ^{13}C signal redistribution by heterotrophic triose phosphate cycling (indicated by prime) (Wieloch *et al.*, 2018). We found that, at least, four ^{13}C signals contribute to the interannual $^{13}C/^{12}C$ variability in tree-ring glucose (Fig. 1B) and proposed the following theories on underlying mechanisms.

We initially proposed the diffusion-rubisco signal is preserved at C-1 to C-3 (Figs. 1B and 2) (Wieloch *et al.*, 2018); although this view is modified here. Additionally, C-1 and C-2 are thought to carry ^{13}C signals due to fractionation at phosphoglucose isomerase (PGI; C-1 and C-2) and glucose-6-phosphate dehydrogenase (G6PD; C-1) (Wieloch *et al.*, 2018, 2022a). Two leaf-level mechanisms of signal introduction were proposed. First, with decreasing carbon assimilation, the plastidial PGI reaction moves from being on the side of fructose 6-phosphate (F6P) towards equilibrium (Fig. 2) (Dietz, 1985). This shift is expected to cause ^{13}C enrichments at C-1 and C-2 of glucose 6-phosphate (G6P) and its derivatives starch and tree-ring glucose (Table 2) (Wieloch *et al.*, 2018). Moreover, shifts towards PGI equilibrium are associated with G6P increases (Dietz, 1985). Increasing G6P is thought to cause G6PD activation and thus increasing flux through the plastidial oxidative pentose phosphate pathway (OPPP) (Cossar *et al.*, 1984; Sharkey & Weise, 2016; Preiser *et al.*, 2019) resulting in additional ^{13}C enrichment at C-1 of G6P and its derivatives (Wieloch *et al.*, 2022a). Reported hydrogen isotope shifts in sunflower leaf starch support these mechanisms (Wieloch *et al.*, 2022a).

Second, the plastidial PGI reaction is usually displaced from equilibrium on the side of F6P whereas the cytosolic PGI reaction is closer to or in equilibrium (Dietz, 1985; Gerhardt *et al.*, 1987; Leidreiter *et al.*, 1995; Schleucher *et al.*, 1999; Szecowka *et al.*, 2013). This is expected to result in $^{13}C/^{12}C$ differences between starch and sucrose at both hexose C-1 and C-2 (Table 2) (Wieloch *et al.*, 2022b). By extension, changes

in the relative contribution of starch to the biosynthesis of tree-ring glucose is expected to contribute to the ^{13}C signals at C-1 and C-2.

In addition to ^{13}C signals at C-1 and C-2, tree-ring glucose samples discussed here carry deuterium signals caused by metabolic processes at H^1 and H^2, which are highly correlated (Wieloch *et al.*, 2022b). These signals were approximated as

$$\varepsilon_{\mathrm{met}} = \frac{(\mathrm{D}_1 + \mathrm{D}_2)/2}{(\mathrm{D}_3 + \mathrm{D}_4 + \mathrm{D}_5 + \mathrm{D}_{6\mathrm{S}} + \mathrm{D}_{6\mathrm{R}})/5} - 1 \qquad (1)$$

where D_i denotes relative deuterium abundances at individual H-C positions (Wieloch *et al.*, 2022a,b). Variability of $\varepsilon_{\mathrm{met}}$ pertaining to glucose H^1 and H^2 was attributed to isotope effects of G6PD ($k_{\mathrm{H}}/k_{\mathrm{D}} = 2.97$) (Hermes *et al.*, 1982) and PGI (Table 2) (Rose & O'Connell, 1961; Wieloch *et al.*, 2022a,b), respectively. Proposedly, G6PD and PGI-dependent metabolic processes in both leaves and tree rings may contribute to $\varepsilon_{\mathrm{met}}$ signal introduction (Wieloch *et al.*, 2022b). Interestingly, Wacker (2022) reported the commonly observed whole-molecule deuterium depletion of leaf starch which derives from glucose H^2 (Schleucher *et al.*, 1999; Wieloch *et al.*, 2022a) is not detectable in nocturnal sucrose. Proposedly, this depletion is either washed out at cytosolic PGI or masked by the vacuolar sucrose pool or deuterium enrichment at other sucrose hydrogen positions. Washout would imply that any $\varepsilon_{\mathrm{met}}$ signal present at leaf-level G6P H^2 is lost to the medium. In this case, the $\varepsilon_{\mathrm{met}}$ signal at tree-ring glucose H^2 and associated ^{13}C signals may originate outside of leaves.

At tree-ring glucose C-4 (Fig. 1B), the diffusion-rubisco ^{13}C signal is thought to be absent due to counteracting fractionation by leaf-cytosolic glyceraldehyde-3-phosphate dehydrogenases (GAPDH; Fig. 2) (Wieloch *et al.*, 2021). Signal removal may involve both changes in 3-phosphoglycerate (PGA) flux into downstream metabolism including the tricarboxylic acid cycle (TCAC) relative to flux into tree-ring glucose and changes of flux through the cytosolic oxidation-reduction cycle (Wieloch, 2021; Wieloch *et al.*, 2021).

The ^{13}C signal at C-5 and C-6 (Fig. 1B) is thought to derive from the postulated (but not yet measured) isotope effects of leaf-level enzymes that modify the carbon double bond in phospho*enol*pyruvate (PEP, Fig. 2) (Wieloch *et al.*, 2022c). This includes enolase, pyruvate kinase (PK), PEPC, and 3-deoxy-D-*arabino*-heptulosonate-7-phosphate synthase (DAHPS), the first enzyme of the shikimate pathway. Bond breakage is thought to favour turnover of ^{12}C isotopologues (Wieloch *et al.*, 2022c). Consequently, increasing relative flux into metabolism downstream of PEP is thought to ^{13}C enrich the PEP double-bond carbons and their derivatives, glucose C-5 and C-6 (Wieloch *et al.*, 2022c). For example, O_3 causes downregulation of rubisco, upregulation of PEPC, and DAHPS expression (Dizengremel, 2001; Janzik *et al.*, 2005; Betz *et al.*, 2009). This is expected to cause increasing relative flux into metabolism downstream of PEP (Wieloch *et*

al., 2022c). Accordingly, we previously found a negative relationship between reconstructed tropospheric O_3 concentration and tree-ring glucose $\Delta_{5\text{-}6}$' (arithmetic average of Δ_5' and Δ_6') (Wieloch *et al.*, 2022c).

By contrast, the diffusion-rubisco signal is not evident at C-5 and C-6 (Wieloch *et al.*, 2022c). This was explained (*inter alia*) by interaction between photorespiration and the TCAC (Fig. 2, Wieloch *et al.*, 2022c). Photorespiration increases with drought increasingly supplying mitochondrial NADH via the glycine decarboxylase complex. Since this NADH can feed oxidative phosphorylation, NADH and $FADH_2$ supply by the TCAC which requires injection of PEP into the TCAC via PK and PEPC may be reduced. This should result in $\Delta_{5\text{-}6}$' increases counteracting drought-induced decreases in diffusion-rubisco discrimination (see above).

The theories of isotope signal introduction outlined above require further testing. They derive from separate analyses of either the Δ_i' or deuterium dataset. However, some reactions exhibit both carbon and hydrogen isotope effects (e.g., G6PD at G6P HC-1, and PGI at G6P HC-2) and should therefore introduce intercorrelated ^{13}C and deuterium signals (suggested terminology: hydro-carbon isotope signals and hydro-carbon isotope fractionation). Combined analysis of intramolecular ^{13}C and deuterium data can, in principle, help to separate those signals from signals introduced by reactions which merely exhibit either carbon or hydrogen isotope effects. Therefore, we here studied the relationships between Δ_i' and ε_{met} and their dependence on multiple environmental parameters. Based on our results, we critically examine and revise existing isotope theory and provide new insights (*inter alia*) into a central open question—whether carbon and hydrogen isotope variability across tree rings derives from leaf-level processes only (as supported by current evidence) or whether processes in the stem contribute as well.

Material and Methods

The Δ_i' and ε_{met} datasets reanalysed here are described in Wieloch *et al.* (2018, 2022b) and in the Supporting Information Notes S1. Data of relative humidity, precipitation (*PRE*), global radiation (*RAD*), sunshine duration (*SD*), and air temperature (*TMP*) are from the climate station Hohe Warte (Vienna, Austria, 48.23° N, 16.35° E, 198 m AMSL) (Klein Tank *et al.*, 2002). Air vapour pressure deficit (*VPD*) was calculated following published procedures (Abtew & Melesse, 2013). Data of the standardised precipitation-evapotranspiration index ($SPEI_i$) calculated for integrated periods of i = 1, 3, 6, 8, 12, 16, 24, 36, 48 months were obtained for 48.25° N, 16.25° E (Fan & van den Dool, 2004; Beguería *et al.*, 2010). The *SPEI* is a multi-scalar drought index approximating soil moisture variability when calculated for short timescales and groundwater variability when calculated for long timescales (Vicente-Serrano *et al.*, 2010). The *RAD* series starts in 1964 while all other climate series start in 1961. Horizontal distances between the tree site and the climate station and grid point are < 15 km. Vertical offsets are small. Hence, climate data and site conditions are expected to be in good agreement. Analytical procedures are described in Notes S1.

Results

Hydro-carbon isotope signals at tree-ring glucose HC-1 and HC-2

Tree-ring glucose of our *Pinus nigra* samples exhibits strongly correlated hydrogen isotope signals at H^1 and H^2 (Wieloch *et al.*, 2022b). These signals occur only after crossing a change point in 1980. Isotope-environment-relationship analyses indicated the trees had likely groundwater access before 1980 preventing changes of the processes introducing these isotope signals. We proposed the signals derive from the hydrogen isotope effects of plastidial and cytosolic G6PD ($k_{\mathrm{H}}/k_{\mathrm{D}} = 2.97$) (Hermes *et al.*, 1982) and PGI (Table 2) (Rose & O'Connell, 1961; Wieloch *et al.*, 2022a) in autotrophic and/or heterotrophic tissue (Fig. 2; 'Introduction') (Wieloch *et al.*, 2022a,b). If this proposal is correct then there should be related signals in Δ_1' and Δ_2' due to the carbon isotope effects of G6PD affecting C-1 ($k_{^{12}\mathrm{C}}/k_{^{13}\mathrm{C}} = 1.0165$) (Hermes *et al.*, 1982) and PGI affecting C-1 and C-2 (Table 2) (Gilbert *et al.*, 2012). Several findings support this hypothesis. First, among all Δ_i' series, Δ_1', $\Delta_{1\text{-}2}$', $\Delta_{1\text{-}3}$', and Δ are not normally distributed (Table S1, negative skew). Second, among these nonnormal series, $\Delta_{1\text{-}2}$', $\Delta_{1\text{-}3}$', and Δ exhibit a change point in 1980 ($\Delta_{1\text{-}2}$': parametric test, $p < 0.001$, nonparametric test, $p < 0.05$; $\Delta_{1\text{-}3}$': parametric test, $p < 0.01$; Δ: parametric test: $p < 0.05$; $n = 31$). Third, 1983 to 1995 average values of Δ_1', Δ_2', $\Delta_{1\text{-}2}$', and Δ are significantly lower than the average values of 1961 to 1980, while the 1983 to 1995 variance is significantly larger (Table S2). By contrast, Δ_3' does not exhibit significant differences in average value or variance between the two periods. Fourth, Δ_1' and Δ_2' data pertaining to 1983 to 1995 are significantly correlated ($r = 0.67$, $p = 0.01$, $n = 13$). Fifth, $\varepsilon_{\mathrm{met}}$ approximates average hydrogen isotope fractionation at glucose H^1 and H^2 caused by metabolic processes (Eq. 1). Using simple linear regression modelling, we found significant negative relationships between the 1983 to 1995 data of $\varepsilon_{\mathrm{met}}$ and Δ_1' as well as Δ_2', but not Δ_3' or any other Δ_i' (Fig. 3, green circles; Δ_1' ~ $\varepsilon_{\mathrm{met}}$: $R^2 = 0.35$, $adjR^2 = 0.29$, $p = 0.03$; Δ_2' ~ $\varepsilon_{\mathrm{met}}$: $R^2 = 0.54$, $adjR^2 = 0.50$, $p = 0.004$; Δ_3' ~ $\varepsilon_{\mathrm{met}}$: $R^2 = 0.21$, $adjR^2 = 0.13$, $p > 0.1$; $n = 13$; Table S3). Our ^{13}C-NMRS data exhibit relatively large measurement errors. Based on estimates of this random error variance, about 88% of the variance in the Δ_1' and Δ_2' data of 1983 to 1995 is systematic variance (Table S4). Hence, about 33% and 57% of the systematic variance in Δ_1' and Δ_2' is explained by processes causing $\varepsilon_{\mathrm{met}}$ variation (and possibly intercorrelated processes) while about 67% and 43%, respectively, go back to other processes. Taken together, carbon and hydrogen isotope signals at glucose HC-1 and HC-2 are significantly associated during 1983 to 1995 but not during 1961 to 1980 (Notes S2). Underlying processes cause concerted ^{13}C and deuterium enrichments (Fig. 3A-B).

Isotope-environment relationships at tree-ring glucose C-1 to C-3

As evident from our previously published hierarchical cluster analysis and Pearson correlation analyses for the whole period 1961 to 1995, Δ_1', Δ_2', and Δ_3' share common variability (Fig. 1B) (Wieloch *et al.*, 2018). Since $\Delta_{1\text{-}2}$' and $\Delta_{1\text{-}3}$' exhibit change points in 1980 (see above and Tables S1-2), we analysed the periods 1961 to 1980 and 1983 to 1995 separately.

During the period 1983 to 1995, Δ_1' and Δ_3' are more closely associated (Fig. 4A; r = 0.87, p = 0.0001, n = 13) than Δ_1' and Δ_2' (r = 0.67, p = 0.01, n = 13). While this contrasts with results for the whole period (Fig. 1B; 1961 to 1995), it is consistent with isotope-climate-relationship patterns for the period 1983 to 1995. Δ_1' and Δ_3' correlate similarly with numerous climate parameters and periods (Table 3; *VPD*, *PRE*, $SPEI_1$ to $SPEI_{16}$, *TMP*, *SD*). By contrast, Δ_2' correlates only with one *VPD* period and several *PRE* periods. A model including ε_{met} and growing season *VPD* as cofactors captures most of the systematic variance in Δ_1' of 88% (Table 4, M1; Table S4). Consistent with the findings above (Fig. 3, Table 3), only ε_{met} but not growing season *VPD* contributes significantly to the corresponding Δ_2' model whereas only growing season *VPD* but not ε_{met} contributes significantly to the Δ_3' model (Table 4, M2-3). Removing insignificant terms, we find that ε_{met} explains 57% of the systematic variance in Δ_2', while growing season *VPD* explains the entire systematic variance in Δ_3' (Table 4, M4-5; Table S4). The effect of *VPD* on Δ_1' is about twice as large as on Δ_3' (Table 4, M1 versus M5) while the effect of ε_{met} on Δ_1' is about half as large as on Δ_2' (M1 versus M4). Intriguingly, Δ_1' and Δ_3' are affected by processes that respond to growing season *VPD*. *VPD*-dependent processes can account for both the clustering and correlation between Δ_1' and Δ_3' data of 1983 to 1995 (Fig. 4A). By contrast, ε_{met} is significantly correlated only with *PRE* (especially March to July *PRE*) but no other climate parameter (Table S5; Table 4, M11). Furthermore, in our Δ_1' and Δ_2' models, ε_{met} can be substituted by March to July *PRE* (Table 4, M1 versus M6, M4 versus M7).

During the period 1961 to 1980, Δ_1', Δ_2', and Δ_3' are not significantly correlated (Fig. 4B). Furthermore, isotope-environment models that work for the period 1983 to 1995 (Table 4, M5-7) do not work for the period 1961 to 1980 (M8-10). Compared to the period 1983 to 1995, we found fewer and weaker isotope-climate correlations (Table 5).

Isotope-environment relationships at tree-ring glucose C-4 to C-6

As evident from our previously published hierarchical cluster analysis and Pearson correlation analyses for the whole period 1961 to 1995, Δ_4', Δ_5', and Δ_6' share common variability, and Δ_5' and Δ_6' are significantly correlated (Fig. 1B; r = 0.61, p < 0.0003, n = 31) (Wieloch *et al.*, 2018). This significant correlation holds for both the early and late study period (Fig. 4). Furthermore, we did not find change points in the Δ_4', Δ_5', and Δ_6' series (see also Tables S1-2). Therefore, we analysed isotope-environment relationships for the whole period. We found that Δ_5' and Δ_6' correlate with numerous climate parameters and periods but most significantly with *RAD* while significant Δ_4'-climate correlations are rare (Table 6). Models including April to September *RAD* and March to October *TMP* as cofactors capture 96% of the systematic variance in $\Delta_{5\text{-}6}$', Δ_5', and Δ_6' of 73%, 66%, and 45%, respectively (Table 7, M1-3; $\Delta_{5\text{-}6}$', $adjR^2$ = 0.70, p = 0.0000001; Δ_5', $adjR^2$ = 0.64, p = 0.000001; Δ_6', $adjR^2$ = 0.43, p = 0.0003; n = 28; Table S4). Based on *RAD* regression slopes (which are better constrained than *TMP* regression slopes), ^{13}C-5 discrimination is about 1.5 times larger than ^{13}C-6 discrimination (Table 7, M2-3). The model works well for the two periods separated by the change point seen in $\Delta_{1\text{-}2}$', $\Delta_{1\text{-}3}$', and Δ (Table 7, M4-5; see above). Furthermore, the model works

reasonably well for Δ_4' considering the relatively low systematic variance in Δ_4' of 38% (Table 7, M6; Table S4). This may explain the weak association between Δ_4' and $\Delta_{5\text{-}6}$' (Fig. 1B).

Discussion

Intramolecular carbon isotope analysis of tree-ring glucose yields information about metabolic variability and water status of both leaves and stems

We found evidence for processes affecting Δ_1' and Δ_3' which respond to *VPD* (Table 4, M1, M3, M5). Intriguingly, we also found evidence for processes simultaneously affecting ε_{met}, Δ_1', and Δ_2' which respond to *PRE* but not *VPD* (Table S5; Table 4, M1, M2, M4, M6, M7, M11). This sensitivity to different hydrological properties may be explained by the fact that stem capacitance can buffer stem water status against changes in *VPD* (McCulloh *et al.*, 2019), whereas leaf water status is tightly coupled to *VPD* (Grossiord *et al.*, 2020). Changes in *PRE* will affect soil water potential and hence both stem and leaf water status. Variability in leaf water status may be impacted more by *VPD* than by soil water status which would explain why *VPD* is the best predictor of the intercorrelated processes affecting Δ_1' and Δ_3'. By contrast, *VPD*-insensitive processes affecting ε_{met}, Δ_1', and Δ_2' may reside in stems. Hence, we propose intramolecular carbon and hydrogen isotope analysis of tree-ring glucose yields information about metabolic variability and water status not only of leaves but also of stems. *PRE*-dependent systemic changes in enzyme expression can be considered as an alternative explanation.

Carbon isotope fractionation mechanisms affecting tree-ring glucose C-1 to C-3

The $\Delta_{1\text{-}2}$' and $\Delta_{1\text{-}3}$' series exhibit change points in 1980, i.e., their frequency distributions do not align with the properties of a single theoretical probability distribution ('Results'; Tables S1-2). Consequently, we investigated the periods 1961 to 1980 and 1983 to 1995 separately. During the period 1983 to 1995, Δ_1' and Δ_3' are significantly intercorrelated (Fig. 4A) and correlate negatively with *VPD* and positively with short-term *SPEI* whereas Δ_2' lacks most of these correlations (Table 3). Furthermore, during this same period, growing season *VPD* accounts for a significant fraction of the systematic variance in Δ_1' and the entire systematic variance in Δ_3' but does not contribute significantly to explaining Δ_2' (Table 4, M1, M2, M5; Table S4). Hence, short-term drought during 1983 to 1995 causes ^{13}C enrichments at tree-ring glucose C-1 and C-3 but not C-2. At C-1, the effect is about twice as large as at C-3 (Table 4, M1 and M5).

As discussed in the previous section, the processes affecting Δ_1' and Δ_3' are likely located in leaves. Qualitatively, drought-induced ^{13}C enrichments at C-1 and C-3 are consistent with the mechanisms of diffusion-rubisco fractionation ('Introduction'). However, diffusion-rubisco fractionation affects all glucose carbon positions equally (Wieloch *et al.*, 2018). Thus, unequal drought responses of Δ_1', Δ_2', and Δ_3' point to fractionations by post-rubisco processes. Assuming the entire systematic variation in Δ_3' derives from diffusion-rubisco fractionation, the following post-rubisco processes may explain observed climate relationships of Δ_1' and Δ_2'.

(i) Flux through the OPPP is regulated at G6PD (Fig. 2). The unidirectional conversion of G6P to 6-phosphogluconolactone catalysed by G6PD proceeds faster with ^{12}C-1 than ^{13}C-1 G6P ($k_{^{12}\mathrm{C}}/k_{^{13}\mathrm{C}} = 1.0165$) (Hermes *et al.*, 1982). Recently, we reported evidence consistent with an increase in relative flux through the plastidial OPPP in response to decreasing p_i (Wieloch *et al.*, 2022a, 2023). In isohydric species such as *Pinus nigra*, p_i decreases with drought due to stomatal closure (McDowell *et al.*, 2008). Thus, increasing relative flux through the plastidial OPPP in response to drought may contribute to the stronger decrease of Δ_1' compared to Δ_3'. The plastidial OPPP is thought to support the regeneration of RuBP when triose phosphates, the substrates for RuBP regeneration in the Calvin-Benson cycle, are in short supply (Wieloch *et al.*, 2023).

(ii) While net carbon assimilation commonly decreases with drought (McDowell *et al.*, 2008), the activity of leaf-cytosolic G6PD reportedly increases (Landi *et al.*, 2016). Drought is also associated with increased concentrations of leaf soluble sugars serving as osmolytes (Bachofen *et al.*, 2017; He *et al.*, 2020). Moreover, it triggers the synthesis of reactive oxygen species (Noctor *et al.*, 2002) increasing the demand for NADPH. Leaf-cytosolic G6PD activity reportedly increases with both soluble sugar concentration (Hauschild & von Schaewen, 2003) and NADPH demand (Fickenscher & Scheibe, 1986). Thus, increasing relative flux through the leaf-cytosolic OPPP in response to drought may contribute to the stronger decrease of Δ_1' compared to Δ_3'. NADPH supplied by the cytosolic OPPP may help to maintain the cellular redox balance (Stincone *et al.*, 2015).

Processes (i) and (ii) should also affect $\varepsilon_{\mathrm{met}}$ at glucose H^1 because of the hydrogen isotope effect of G6PD ($k_{\mathrm{H}}/k_{\mathrm{D}} = 2.97$) (Hermes *et al.*, 1982). However, we found no relationship between $\varepsilon_{\mathrm{met}}$ at glucose H^1 and growing season *VPD* (Table S6). Hence, either G6PD-related processes are not the main drivers of *VPD*-dependent change in Δ_1' or the corresponding $\varepsilon_{\mathrm{met}}$ signal was washed out after introduction. Washout may occur during equilibration of F6P with mannose 6-phosphate by phosphomannose isomerase (Topper, 1957).

(iii) PGI reversibly converts F6P into G6P (Fig. 2). Under nonstress conditions, the plastidial PGI reaction is strongly displaced from equilibrium on the side of F6P (Dietz, 1985; Gerhardt *et al.*, 1987; Kruckeberg *et al.*, 1989; Schleucher *et al.*, 1999; Wieloch *et al.*, 2022a; Wieloch, 2022). With decreasing p_i, however, the reaction moves towards equilibrium (Dietz, 1985; Wieloch *et al.*, 2022a). This shift is accompanied by ^{13}C increases at C-1 and C-2 of G6P which will be transmitted to downstream derivatives such as starch and tree-ring glucose (Table 2) (Wieloch *et al.*, 2018). Thus, a shift of the PGI reaction in response to increasing drought (decreasing p_i) is in line with the stronger decrease of Δ_1' compared to Δ_3' but not with the apparent absence of the diffusion-rubisco signal from Δ_2'. That said, the relative contribution of plastidial G6P and its

isotope composition to downstream metabolism may vary. For example, in leaves of *Phaseolus vulgaris*, the ratio of sucrose-to-starch carbon partitioning increases steeply with decreasing p_i (Sharkey *et al.*, 1985).

(iv) Under illumination, plastidial F6P is used for both RuBP regeneration via transketolase and starch biosynthesis via PGI (Fig. 2). Increasing drought promotes photorespiration resulting in increasing RuBP regeneration relative to carbon export from the Calvin-Benson cycle into sinks such as starch. Furthermore, under drought, the PGI reaction operates closer to equilibrium; see process (iii). Combinedly, this should result in increasing ^{13}C abundance at C-1 and decreasing ^{13}C abundance at C-2 of plastidial G6P and downstream derivatives. Thus, this mechanism may contribute to the stronger drought-induced decrease of Δ_1' compared to Δ_3' and the apparent absence of the diffusion-rubisco signal in Δ_2'.

(v) Under illumination, plastidial G6P can enter either the OPPP via G6PD or starch biosynthesis via phosphoglucomutase (Fig. 2). Increasing drought can cause increasing relative G6P flux into the plastidial OPPP; see process (i). Furthermore, under drought, the plastidial PGI reaction is likely operating closer to equilibrium; see process (iii). Combinedly, this should result in decreasing ^{13}C abundance at C-1 and increasing ^{13}C abundance at C-2 of remaining G6P and downstream derivatives. Thus, this mechanism contrasts with the stronger drought-induced decrease of Δ_1' compared to Δ_3' and the apparent absence of the diffusion-rubisco signal in Δ_2'. Similar mechanisms may apply to the cytosol where increasing drought can cause increasing relative flux into the cytosolic OPPP; see process (ii).

(vi) In natural systems, leaf dark respiration increases with drought (Schmiege *et al.*, 2023 and references therein) while carbon assimilation decreases (McDowell *et al.*, 2008). When the PGI reaction is in equilibrium, F6P C-1 is ^{13}C depleted while F6P C-2 is ^{13}C enriched relative to the corresponding G6P positions (Table 2). Consequently, increasing relative F6P flux into dark respiration may result in increasing ^{13}C abundance at C-1 and decreasing ^{13}C abundance at C-2 of G6P. Hence, this mechanism may contribute to the stronger drought-induced decrease of Δ_1' compared to Δ_3' and the apparent absence of the diffusion-rubisco signal in Δ_2'.

VPD contributes significantly to only two out of the six Δ_i' models (Tables 4 and 7). This is surprising because diffusion-rubisco fractionation is expected to affect all glucose carbon positions equally and in a *VPD*-dependent manner (Wieloch *et al.*, 2018). It is impossible to tell whether the diffusion-rubisco signal has been removed by post-rubisco fractionation from four glucose carbon positions (C-2, C-4, C-5, C-6) or whether it has not been strongly introduced to begin with. In the latter case, the *VPD*-dependence of Δ_3' would go back to post-rubisco fractionation processes and post-rubisco fractionation processes that have been invoked to explain the absence of the diffusion-rubisco signal from C-2, C-4, C-5, and C-6 would not occur.

Hydro-carbon isotope fractionation mechanisms affecting tree-ring glucose HC-1 and HC-2

Previously, we found a change point in ε_{met} in 1980 (Wieloch *et al.*, 2022b). Here, we found the same change point in $\Delta_{1\text{-}2}$' ('Results'). Consistent with this, Δ_1' and Δ_2' data of 1983 to 1995 exhibit a significantly lower average value and a significantly larger variance than those of 1961 to 1980 (Tables S1-2). Furthermore, Δ_1' and Δ_2' are significantly correlated during 1983 to 1995 (Fig. 4B) but not during 1961 to 1980 (Fig. 4A), and ε_{met} accounts for a significant fraction of the variance of both Δ_1' and Δ_2' during 1983 to 1995 (Table 4, M1, M4; Figs. 3A-B). In Δ_2', the ε_{met} effect is about twice as large as in Δ_1'. Processes affecting ε_{met}, Δ_1', and Δ_2' simultaneously respond to *PRE* but not *VPD* (Table S5; Table 4, M1, M2, M4, M6, M7, M11). Δ_1' and Δ_2' respond to March to July *PRE* during 1983 to 1995 but not during 1961 to 1980 (Table 4, M9-10). Previously, we reported evidence suggesting that the groundwater table before 1980 was high enough to prevent metabolic changes causing ε_{met} variation (Wieloch *et al.*, 2022b). By extension, this should also explain the properties of Δ_1' and Δ_2' listed above. That is, since the trees had access to groundwater during the period 1961 to 1980 metabolic shifts that could cause intercorrelated variation in ε_{met}, Δ_1', and Δ_2' were not induced.

Processes causing intercorrelated variation in ε_{met}, Δ_1', and Δ_2' are probably located in the stem (see the first section of the 'Discussion'). The ε_{met} signal is present at glucose H^1 and, considerably more strongly, at H^2 (range: 64‰ and 240‰, respectively; 1983 to 1995). In the biochemical pathway leading to tree-ring cellulose, PGI is the last enzyme acting on precursors of glucose H^2 (Fig. 2). With each conversion by PGI, there is a probability for hydrogen exchange with the medium of about 30% (Fedtke, 1969; Noltmann, 1972). Thus, if the PGI reaction is in equilibrium, then any deuterium signal at G6P H^2 will be washed out. Among all glucose H-C positions, the deuterium abundance at H^2 is neither exceptionally high nor low during 1961 to 1980 whereas it is exceptionally high (and exceptionally variable) during 1983 to 1995 (Fig. 5). This indicates that the PGI reaction was close to or in equilibrium during 1961 to 1980 but displaced from equilibrium on the side of G6P during 1983 to 1995 (Table 2). Additionally, shifts of the PGI reaction away from equilibrium towards the side of G6P should also cause Δ_1' and Δ_2' decreases, and Δ_2' should decrease 3 times more than Δ_1' (Table 2). Consistent with this, we found negative relationships between ε_{met} and Δ_1', as well as Δ_2' (Table 4, M1 and M4). However, Δ_2' decreases only 1.88 times more than Δ_1' although this best estimate is associated with a relatively large error (SE interval: 1.04 to 3.45). Nevertheless, the offset from 3 is likely explained by increasing relative flux through the plastidial and/or cytosolic OPPP accompanying the putative PGI reaction shift (Fig. 2). This is because G6P to 6-phosphogluconolactone conversion by G6PD exhibit ^{13}C and D isotope effects ($k_{^{12}C}/k_{^{13}C} = 1.0165, k_H/k_D = 2.97$) (Hermes *et al.*, 1982). Hence, increasing relative OPPP flux is associated with decreasing ^{13}C discrimination at G6P C-1 (Δ_1' decreases) and increasing deuterium abundance at G6P H^1. This is consistent with the apparently decreased PGI effects ratio (1.88 instead of 3) and ε_{met} increases at glucose H^1 during 1983 to 1995 of up to 64‰ (Fig. 5), respectively.

Sucrose translocated from leaves can be split into UDP-glucose and fructose via sucrose synthase or glucose and fructose via invertase (Fig. 2). UDP-glucose entering tree-ring cellulose biosynthesis directly via sucrose synthase is protected from isotope fractionation by PGI and G6PD. However, in stems of juvenile *Quercus petraea* and *Picea abies*, at least 79% and 43% of the precursors of tree-ring glucose went through PGI catalysis, respectively (Augusti *et al.*, 2006). Theoretically, shifts of the PGI reaction away from equilibrium towards the side of G6P can cause ε_{met} increases at glucose H^2 of up to 611‰ (Notes S3, hydrogen exchange with the medium not considered). With 43% and 79% of all precursors of tree-ring glucose undergoing PGI catalysis, ε_{met} increases at glucose H^2 of up to 263‰ and 483‰ are possible, respectively. Thus, the PGI-related fractionation mechanism proposed here can potentially cause the previously reported ε_{met} increases at glucose H^2 of up to 240‰ (Wieloch *et al.*, 2022b). Shifts in sucrose cleavage by sucrose synthase versus invertase may exert additional control on the ε_{met} signal at glucose H^2.

Based on results and interpretations presented above, decreasing stem moisture is associated with both increasing OPPP flux and a shift of the PGI reaction away from equilibrium towards the side of G6P corresponding to low relative F6P concentration. We propose these concerted shifts may ensure redox homeostasis and balanced substrate supply to glycolysis as follows. In heterotrophic tissue, NADPH from the OPPP is believed to be central for maintaining redox homeostasis (Fig. 2) (Stincone *et al.*, 2015). Flux through the OPPP is regulated at G6PD. Heterotrophic G6PD activity reportedly increases with drought (Liu *et al.*, 2013; Wang *et al.*, 2016, 2020), oxidative load (Wang *et al.*, 2016, 2020; Li *et al.*, 2020), NADPH demand (Wendt *et al.*, 2000; Esposito *et al.*, 2001; Castiglia *et al.*, 2015), and abscisic acid concentration (Cardi *et al.*, 2011; Wang *et al.*, 2016). Decreasing stem moisture may cause increasing OPPP flux via increasing abscisic acid concentration (Brunetti *et al.*, 2020), and possibly increasing oxidative load increasing the demand for NADPH. In turn, increasing OPPP flux results in increasing supply of pentose phosphates which may feed into glycolysis via the reductive part of the pentose phosphate pathway (Fig. 2). This would reduce the demand for glycolytic substrates supplied via PGI. The shift of the PGI reaction away from equilibrium towards the side of G6P may reflect this decreased demand and result from PGI downregulation by intermediates of the pentose phosphate pathway such as erythrose 4-phosphate, ribulose 5-phosphate, and 6-phosphogluconate (Parr, 1956; Grazi *et al.*, 1960; Salas *et al.*, 1965). Furthermore, relative changes in G6P-to-F6P supply versus consumption may contribute to the shift of the PGI reaction. For instance, while starch storage consumes G6P, remobilisation supplies G6P (Noronha *et al.*, 2018). Under drought, the storage-to-remobilisation balance may tilt towards remobilisation (Mitchell *et al.*, 2013; Thalmann & Santelia, 2017; Tsamir-Rimon *et al.*, 2021). Consequently, the PGI reaction may move towards the side of G6P. Similarly, we previously reported below-average tree-ring widths for years in which the PGI reaction is on the side of G6P (Wieloch *et al.*, 2022b). In these years, G6P consumption by growth may have been reduced while F6P consumption by downstream metabolism may have been maintained.

1961 to 1980: A period of homeostasis with respect to processes affecting Δ_1', Δ_2', Δ_3', and ε_{met}

During 1961 to 1980, Δ_1', Δ_2', and Δ_3' are not significantly correlated (Fig. 4b). This contrasts with the period 1983 to 1995 (Fig. 4a). Furthermore, relationships of Δ_1' and Δ_3' with *VPD* and Δ_1' and Δ_2' with *PRE* observed during 1983 to 1995 are largely absent during 1961 to 1980 (Tables 3-5) even though there is no difference in the degree of *VPD* and *PRE* variability between the two periods (Fig. S1). However, like $\Delta_{1\text{-}2}$' and $\Delta_{1\text{-}3}$', ε_{met} exhibits a change point in 1980 and responds to *PRE* after but not before 1980 (Wieloch *et al.*, 2022b). This sensitivity change was attributed to long-term drought developing over the study period proposedly causing groundwater depletion below a critical level in 1980. By extension, the groundwater decrease might also explain the insensitivity of Δ_1' and Δ_3' to *VPD* and Δ_1' and Δ_2' to *PRE* during 1961 to 1980 and their sensitivity from 1983 onwards. Thus, leaf-level processes affecting Δ_1', Δ_2', and Δ_3' and stem-level processes affecting Δ_1', Δ_2', and ε_{met} can apparently maintain homeostasis despite changing atmospheric conditions if the trees have access to groundwater.

Carbon isotope fractionation mechanisms affecting tree-ring glucose C-5 and C-6

No change points were detected in Δ_5' and Δ_6' ('Results'; Tables S1-2). Furthermore, Δ_5' and Δ_6' remain significantly correlated across the entire study period (Figs. 1B and 4A-B), and *RAD* is the most influential environmental cofactor (Table 6). Models including *RAD* and *TMP* as cofactors capture most of the systematic variance in $\Delta_{5\text{-}6}$', Δ_5', and Δ_6' (Table 7, M1-3; Table S4). These relationships hold for both the early and late study period (Table 7, M4-5) with Δ_5' effects being about 1.5-fold larger than Δ_6' effects (M2 versus M3, SE interval: 1.1 to 2.28).

Previously, we reported a negative relationship between tree-ring glucose $\Delta_{5\text{-}6}$' and reconstructed tropospheric O_3 concentration ('Introduction', Wieloch *et al.*, 2022c). Light stimulates tropospheric O_3 formation (Lu *et al.*, 2019). This may explain the negative relationship between tree-ring glucose $\Delta_{5\text{-}6}$' and *RAD* reported here (Table 7, M1-3). Furthermore, we previously explained the absence of the diffusion-rubisco signal from glucose C-5 and C-6 (*inter alia*) by interaction between photorespiration and the TCAC ('Introduction', Wieloch *et al.*, 2022c). As *TMP* increases, photorespiration increases more than photosynthesis (Long, 1991). This may result in decreased flux of PEP into the TCAC ('Introduction') and explain the positive relationship between tree-ring glucose $\Delta_{5\text{-}6}$' and *TMP* reported here (Table 7, M1-3).

Carbon isotope fractionation mechanisms affecting tree-ring glucose C-4

As for Δ_5' and Δ_6', no change point was detected in Δ_4' ('Results'; Tables S1-2). Considering the entire study period, Δ_4' is weakly associated with $\Delta_{5\text{-}6}$' (Fig. 1B). Consistent with this, the $\Delta_{5\text{-}6}$'-climate model works reasonably well for Δ_4' considering the relatively low systematic variance in Δ_4' of 38% (Table 7, M1 and M6; Table S4). Introduction of the Δ_4' and $\Delta_{5\text{-}6}$' signals proposedly involves leaf-level consumption of PGA and PEP by downstream metabolism, respectively (Wieloch *et al.*, 2021, 2022c). Since PGA is a precursor

of PEP (Fig. 2), our previously proposed theories of signal introduction are in line with the observation that Δ_4', Δ_5' and Δ_6' are associated and respond to the same environmental parameters.

Conclusions and future directions

Combined analysis of Δ_i' and ε_{met} provided new insights into plant isotope fractionation. First, isotope fractionation beyond leaves is usually considered to be constant for any given species (Roden *et al.*, 2000; Gagen *et al.*, 2022). Our results suggest, however, that a significant part of the carbon and hydrogen isotope variation in tree-ring glucose originates in stems from processes affecting Δ_1', Δ_2', and ε_{met} simultaneously. Second, we show that combined analysis of carbon and hydrogen isotope data enables deconvolution of carbon isotope signals. Third, the diffusion-rubisco signal was shown previously to be absent from tree-ring glucose C-4 to C-6 (Wieloch *et al.*, 2021, 2022c) but believed to be present at C-1 to C-3 (Wieloch *et al.*, 2018). Here, we found that the signal is also absent from C-2. Since the diffusion-rubisco signal is thus absent from four out of six glucose carbon positions, the question arises whether it was already below the detection level on introduction. In this case, *VPD*-dependent signals detected in Δ_1' and Δ_3' would originate entirely from post-rubisco processes. Fourth, we previously reported a change point in ε_{met} in 1980 which was attributed to the assumed crossing of a physiologically relevant groundwater threshold (Wieloch *et al.*, 2022b). Here, we found the same change point in $\Delta_{1\text{-}3}$'. It divides a period of homeostasis with respect to processes affecting Δ_1', Δ_2', Δ_3', and ε_{met} (1961 to 1980) from a period where these processes vary in response to environmental conditions (1983 to 1995). Fifth, we previously reported a relationship between $\Delta_{5\text{-}6}$' and reconstructed tropospheric O_3 concentration (Wieloch *et al.*, 2022c). Here, we report $\Delta_{5\text{-}6}$' relationships with *RAD* and *TMP* which are consistent with previously proposed fractionation mechanisms. Sixth, Δ_1' and Δ_2' vary with *PRE*, Δ_1' and Δ_3' vary with *VPD*, and Δ_5' and Δ_6' vary with *RAD* and *TMP* (Table 4). Furthermore, $\Delta_{1\text{-}2}$' and $\Delta_{1\text{-}3}$' exhibit change points marking transitions in long-term moisture (groundwater) conditions. Thus, intramolecular carbon isotope analysis has an extraordinary potential for climate reconstruction. Seventh, to provide a basis for follow-up studies, we propose comprehensive theories on mechanisms underlying Δ_1', Δ_2', Δ_3', and ε_{met} variability. Note, phosphomannose-isomerase-related mechanisms are not detailed here but may contribute to isotope signal introduction.

Understanding isotope fractionation mechanisms is central for retrospective studies of plant physiology and climate based on tree-ring isotope data, and there is considerable room for improvement as shown above. Research in several largely unexploited areas is needed to make progress. First, there is a basic need for more *in vitro* data on intramolecular isotope effects of enzyme reactions including the reactions catalysed by triosephosphate isomerase, transketolase, PEPC, PK, and DAHPS. Second, intramolecular isotope analyses of leaf metabolites including starch and sucrose from both controlled and natural environments are needed to generate a baseline for mechanistic studies of isotope fractionation along the pathway from leaves to wood. Additionally, intramolecular isotope analysis of metabolites from wood slices acclimated to different ambient conditions (e.g., wet versus dry, varying sucrose supply) will be insightful. Third, combined

analysis of intramolecular ^{13}C and deuterium data can help to separate isotope signals. Fourth, genetic modification of key enzymes may help to test proposed isotope fractionation mechanisms *in vivo*. Fifth, intramolecular isotope fractionation affecting tree-ring glucose is complex (see above). Software programs such as QIRN enable the convenient simulation of natural isotope abundances in complex metabolic networks (Mueller *et al.*, 2022). If expanded, these programs may help to extract metabolic information from intramolecular tree-ring isotope data. This would require routines enabling control of relative flux at metabolic branchpoints by optimising regressions between (i) relative branchpoint flux and environmental parameters and (ii) simulated and observed isotope data. In summary, intramolecular isotope analysis has an enormous potential to advance our knowledge about isotope fractionation mechanisms, plant ecophysiology, and paleoclimatology.

Acknowledgements

TW's work was carried out with funding from "Formas - a Swedish Research Council for Sustainable Development" (2022-02833, Grant recipient: TW). MHP's work was supported by the Swiss National Science Foundation (205492).

Author Contributions

Conceptualisation: TW; Investigation: TW with input from all authors; Visualization: TW; Development of isotope theory: TW; Project administration: TW; Writing – original draft: TW with input from all authors.

Competing interests

None declared.

Data availability

The authors declare that the data supporting the findings of this study are available within the paper and its supplementary information files.

References

Abtew W, Melesse AM. **2013**. Chapter 5 - Vapor pressure calculation methods. In: Evaporation and Evapotranspiration. Springer Verlag, 53–62.

Augusti A, Betson TR, Schleucher J. **2006**. Hydrogen exchange during cellulose synthesis distinguishes climatic and biochemical isotope fractionations in tree rings. *New Phytologist* **172**: 490–499.

Bachofen C, Moser B, Hoch G, Ghazoul J, Wohlgemuth T. **2017**. No carbon 'bet hedging' in pine seedlings under prolonged summer drought and elevated CO_2. *Journal of Ecology*: 1–16.

Badeck FW, Tcherkez G, Nogues S, Piel C, Ghashghaie J. **2005**. Post-photosynthetic fractionation of stable carbon isotopes between plant organs-a widespread phenomenon. *Rapid Communications in Mass Spectrometry* **19**: 1381–1391.

Beguería S, Vicente-Serrano SM, Angulo-Martínez M. **2010**. A multiscalar global drought dataset: The SPEIbase. *Bulletin of the American Meteorological Society* **91**: 1351–1356.

Betz GA, Gerstner E, Stich S, Winkler B, Welzl G, Kremmer E, Langebartels C, Heller W, Sandermann H, Ernst D. **2009**. Ozone affects shikimate pathway genes and secondary metabolites in saplings of European beech (*Fagus sylvatica* L.) grown under greenhouse conditions. *Trees* **23**: 539–553.

Brunetti C, Savi T, Nardini A, Loreto F, Gori A, Centritto M. **2020**. Changes in abscisic acid content during and after drought are related to carbohydrate mobilization and hydraulic recovery in poplar stems. *Tree Physiology* **40**: 1043–1057.

Cardi M, Chibani K, Cafasso D, Rouhier N, Jacquot J-P, Esposito S. **2011**. Abscisic acid effects on activity and expression of barley (*Hordeum vulgare*) plastidial glucose-6-phosphate dehydrogenase. *Journal of Experimental Botany* **62**: 4013–4023.

Castiglia D, Cardi M, Landi S, Cafasso D, Esposito S. **2015**. Expression and characterization of a cytosolic glucose 6 phosphate dehydrogenase isoform from barley (*Hordeum vulgare*) roots. *Protein Expression and Purification* **112**: 8–14.

Cernusak LA, Tcherkez G, Keitel C, Cornwell WK, Santiago LS, Knohl A, Barbour MM, Williams DG, Reich PB, Ellsworth DS, *et al.* 2009. Why are non-photosynthetic tissues generally ^{13}C enriched compared with leaves in C_3 plants? Review and synthesis of current hypotheses. *Functional Plant Biology* **36**: 199–213.

Cossar JD, Rowell P, Stewart WDP. **1984**. Thioredoxin as a modulator of glucose-6-phosphate dehydrogenase in a N_2-fixing cyanobacterium. *Microbiology* **130**: 991–998.

Craig H. **1953**. The geochemistry of the stable carbon isotopes. *Geochimica Et Cosmochimica Acta* **3**: 53–92.

Dietz K-J. **1985**. A possible rate-limiting function of chloroplast hexosemonophosphate isomerase in starch synthesis of leaves. *Biochimica et Biophysica Acta* **839**: 240–248.

Dizengremel P. **2001**. Effects of ozone on the carbon metabolism of forest trees. *Plant Physiology and Biochemistry* **39**: 729–742.

Eicks M, Maurino V, Knappe S, Flügge U-I, Fischer K. **2002**. The plastidic pentose phosphate translocator represents a link between the cytosolic and the plastidic pentose phosphate pathways in plants. *Plant Physiology* **128**: 512–522.

Esposito S, Carfagna S, Massaro G, Vona V, Di Martino Rigano V. **2001**. Glucose-6-phosphate dehydrogenase in barley roots: kinetic properties and localisation of the isoforms. *Planta* **212**: 627–634.

Evans JR, Farquhar GD, Sharkey TD, Berry JA. **1986**. Carbon isotope discrimination measured concurrently with gas exchange to investigate CO_2 diffusion in leaves of higher plants. *Australian Journal of Plant Physiology* **13**: 281–292.

Fan Y, van den Dool H. **2004**. Climate Prediction Center global monthly soil moisture data set at 0.5° resolution for 1948 to present. *Journal of Geophysical Research: Atmospheres* **109**.

Farquhar GD. **1983**. On the nature of carbon isotope discrimination in C_4 species. *Australian Journal of Plant Physiology* **10**: 205–226.

Farquhar GD, O'Leary MH, Berry JA. **1982**. On the relationship between carbon isotope discrimination and the intercellular carbon dioxide concentration in leaves. *Australian Journal of Plant Physiology* **9**: 121–137.

Farquhar GD, Richards RA. **1984**. Isotopic composition of plant carbon correlates with water-use efficiency of wheat genotypes. *Australian Journal of Plant Physiology* **11**: 539–552.

Fedtke C. **1969**. Intramolecular hydrogen transfer in isomerisation reactions of sugar phosphates in the Calvin cycle. In: Metzner H, ed. Progress in Photosynthesis Research. Tübingen, 1597–1603.

Fickenscher K, Scheibe R. **1986**. Purification and properties of the cytoplasmic glucose-6-phosphate dehydrogenase from pea leaves. *Archives of Biochemistry and Biophysics* **247**: 393–402.

Gagen M, Battipaglia G, Daux V, Duffy J, Dorado-Liñán I, Hayles LA, Martínez-Sancho E, McCarroll D, Shestakova TA, Treydte K. **2022**. Climate signals in stable isotope tree-ring records. In: Siegwolf RTW, Brooks JR, Roden J, Saurer M, eds. Stable isotopes in tree tings: Inferring physiological, climatic and environmental responses. Cham: Springer International Publishing, 537–579.

Gerhardt R, Stitt M, Heldt HW. **1987**. Subcellular metabolite levels in spinach leaves: Regulation of sucrose synthesis during diurnal alterations in photosynthetic partitioning. *Plant Physiology* **83**: 399–407.

Gilbert A, Robins RJ, Remaud GS, Tcherkez G. **2012**. Intramolecular ^{13}C pattern in hexoses from autotrophic and heterotrophic C_3 plant tissues. *Proceedings of the National Academy of Sciences of the United States of America* **109**: 18204–18209.

Grazi E, De Flora A, Pontremoli S. **1960**. The inhibition of phosphoglucose isomerase by D-erythrose 4-phosphate. *Biochemical and Biophysical Research Communications* **2**: 121–125.

Grossiord C, Buckley TN, Cernusak LA, Novick KA, Poulter B, Siegwolf RTW, Sperry JS, McDowell NG. **2020**. Plant responses to rising vapor pressure deficit. *New Phytologist* **226**: 1550–1566.

Hauschild R, von Schaewen A. **2003**. Differential regulation of glucose-6-phosphate dehydrogenase isoenzyme activities in potato. *Plant Physiology* **133**: 47–62.

He W, Liu H, Qi Y, Liu F, Zhu X. **2020**. Patterns in nonstructural carbohydrate contents at the tree organ level in response to drought duration. *Global Change Biology* **26**: 3627–3638.

Hermes JD, Roeske CA, O'Leary MH, Cleland WW. **1982**. Use of multiple isotope effects to determine enzyme mechanisms and intrinsic isotope effects. Malic enzyme and glucose 6-phosphate dehydrogenase. *Biochemistry* **21**: 5106–5114.

Hobbie EA, Werner RA. **2004**. Intramolecular, compound-specific, and bulk carbon isotope patterns in C_3 and C_4 plants: a review and synthesis. *New Phytologist* **161**: 371–385.

Janzik I, Preiskowski S, Kneifel H. **2005**. Ozone has dramatic effects on the regulation of the prechorismate pathway in tobacco (*Nicotiana tabacum* L. cv. Bel W3). *Planta* **223**: 20–27.

Klein Tank AMG, Wijngaard JB, Können GP, Böhm R, Demarée G, Gocheva A, Mileta M, Pashiardis S, Hejkrlik L, Kern-Hansen C, *et al.* 2002. Daily dataset of 20th-century surface air temperature and precipitation series for the European Climate Assessment. *International Journal of Climatology* **22**: 1441–1453.

Kruckeberg AL, Neuhaus HE, Feil R, Gottlieb LD, Stitt M. **1989**. Decreased-activity mutants of phosphoglucose isomerase in the cytosol and chloroplast of *Clarkia xantiana*. *The Biochemical Journal* **261**: 457–467.

Landi S, Nurcato R, De Lillo A, Lentini M, Grillo S, Esposito S. **2016**. Glucose-6-phosphate dehydrogenase plays a central role in the response of tomato (*Solanum lycopersicum*) plants to short and long-term drought. *Plant Physiology and Biochemistry* **105**: 79–89.

Leavitt SW, Roden J. **2022**. Isotope dendrochronology: Historical perspective. In: Siegwolf RTW, Brooks JR, Roden J, Saurer M, eds. Stable isotopes in tree rings: Inferring physiological, climatic and environmental Responses. Cham: Springer International Publishing, 3–20.

Leidreiter K, Kruse A, Heineke D, Robinson DG, Heldt H-W. **1995**. Subcellular volumes and metabolite concentrations in potato (*Solanum tuberosum* cv. Désirée) leaves. *Botanica Acta* **108**: 439–444.

Li C, Wei M, Ge Y, Zhao J, Chen Y, Hou J, Cheng Y, Chen J, Li J. **2020**. The role of glucose-6-phosphate dehydrogenase in reactive oxygen species metabolism in apple exocarp induced by acibenzolar-S-methyl. *Food Chemistry* **308**: 125663.

Liu J, Wang X, Hu Y, Hu W, Bi Y. **2013**. Glucose-6-phosphate dehydrogenase plays a pivotal role in tolerance to drought stress in soybean roots. *Plant Cell Reports* **32**: 415–29.

Long SP. **1991**. Modification of the response of photosynthetic productivity to rising temperature by atmospheric CO_2 concentrations: Has its importance been underestimated? *Plant, Cell & Environment* **14**: 729–739.

Lu X, Zhang L, Shen L. **2019**. Meteorology and climate influences on tropospheric ozone: a review of natural sources, chemistry, and transport patterns. *Current Pollution Reports* **5**: 238–260.

McCulloh KA, Domec J-C, Johnson DM, Smith DD, Meinzer FC. **2019**. A dynamic yet vulnerable pipeline: Integration and coordination of hydraulic traits across whole plants. *Plant, Cell & Environment* **42**: 2789–2807.

McDowell N, Pockman WT, Allen CD, Breshears DD, Cobb N, Kolb T, Plaut J, Sperry J, West A, Williams DG, *et al.* 2008. Mechanisms of plant survival and mortality during drought: why do some plants survive while others succumb to drought? *New Phytologist* **178**: 719–739.

Mitchell PJ, O'Grady AP, Tissue DT, White DA, Ottenschlaeger ML, Pinkard EA. **2013**. Drought response strategies define the relative contributions of hydraulic dysfunction and carbohydrate depletion during tree mortality. *New Phytologist* **197**: 862–872.

Mueller EP, Wu F, Sessions AL. **2022**. Quantifying Isotopologue Reaction Networks (QIRN): A modelling tool for predicting stable isotope fractionations in complex networks. *Chemical Geology* **610**: 121098.

Noctor G, Veljovic-Jovanovic S, Driscoll S, Novitskaya L, Foyer CH. **2002**. Drought and oxidative load in the leaves of C_3 plants: a predominant role for photorespiration? *Annals of Botany* **89**: 841–850.

Noltmann EA. **1972**. 9 Aldose-ketose isomerases. In: Boyer PD, ed. The Enzymes. Academic Press, 271–354.

Noronha H, Silva A, Dai Z, Gallusci P, Rombolà AD, Delrot S, Gerós H. **2018**. A molecular perspective on starch metabolism in woody tissues. *Planta* **248**: 559–568.

Parr CW. **1956**. Inhibition of phosphoglucose isomerase. *Nature* **178**: 1401.

Preiser AL, Fisher N, Banerjee A, Sharkey TD. **2019**. Plastidic glucose-6-phosphate dehydrogenases are regulated to maintain activity in the light. *Biochemical Journal* **476**: 1539–1551.

Roden JS, Lin G, Ehleringer JR. **2000**. A mechanistic model for interpretation of hydrogen and oxygen isotope ratios in tree-ring cellulose. *Geochimica et Cosmochimica Acta* **64**: 21–35.

Roeske CA, O'Leary MH. **1984**. Carbon isotope effects on the enzyme-catalyzed carboxylation of ribulose bisphosphate. *Biochemistry* **23**: 6275–6284.

Rose IA, O'Connell EL. **1961**. Intramolecular hydrogen transfer in the phosphoglucose isomerase reaction. *The Journal of Biological Chemistry* **236**: 3086–3092.

Salas M, Vinuela E, Sols A. **1965**. Spontaneous and enzymatically catalyzed anomerization of glucose 6-phosphate and anomeric specificity of related enzymes. *Journal of Biological Chemistry* **240**: 561–568.

Schleucher J, Vanderveer P, Markley JL, Sharkey TD. **1999**. Intramolecular deuterium distributions reveal disequilibrium of chloroplast phosphoglucose isomerase. *Plant, Cell and Environment* **22**: 525–533.

Schmiege SC, Heskel M, Fan Y, Way DA. **2023**. It's only natural: Plant respiration in unmanaged systems. *Plant Physiology* **192**: 710–727.

Sharkey TD, Berry JA, Raschke K. **1985**. Starch and sucrose synthesis in *Phaseolus vulgaris* as affected by light, CO_2, and abscisic acid. *Plant Physiology* **77**: 617–620.

Sharkey TD, Weise SE. **2016**. The glucose 6-phosphate shunt around the Calvin–Benson cycle. *Journal of Experimental Botany* **67**: 4067–4077.

Stincone A, Prigione A, Cramer T, Wamelink MM, Campbell K, Cheung E, Olin-Sandoval V, Gruning N, Kruger A, Tauqeer Alam M, *et al.* 2015. The return of metabolism: biochemistry and physiology of the pentose phosphate pathway. *Biological Reviews Cambridge Philosphical Society* **90**: 927–963.

Szecowka M, Heise R, Tohge T, Nunes-Nesi A, Vosloh D, Huege J, Feil R, Lunn J, Nikoloski Z, Stitt M, *et al.* 2013. Metabolic fluxes in an illuminated *Arabidopsis* rosette. *The Plant Cell* **25**: 694–714.

Thalmann M, Santelia D. **2017**. Starch as a determinant of plant fitness under abiotic stress. *New Phytologist* **214**: 943–951.

Topper YJ. **1957**. On the mechanism of action of phosphoglucose isomerase and phosphomannose isomerase. *Journal of Biological Chemistry* **225**: 419–425.

Tsamir-Rimon M, Ben-Dor S, Feldmesser E, Oppenhimer-Shaanan Y, David-Schwartz R, Samach A, Klein T. **2021**. Rapid starch degradation in the wood of olive trees under heat and drought is permitted by three stress-specific beta amylases. *New Phytologist* **229**: 1398–1414.

Ubierna N, Holloway-Phillips M-M, Farquhar GD. **2022**. Scaling from fluxes to organic matter: interpreting ^{13}C isotope ratios of plant material using flux models. *New Phytologist* **236**: 2003–2008.

Vicente-Serrano SM, Beguería S, López-Moreno JI. **2010**. A multiscalar drought index sensitive to global warming: The standardized precipitation evapotranspiration index. *Journal of Climate* **23**: 1696–1718.

Wacker A. **2022**. Leaf sucrose shows no nighttime ^{2}H-depletion despite the degradation of strongly ^{2}H-depleted starch.

Wang X, Ruan M, Wan Q, He W, Yang L, Liu X, He L, Yan L, Bi Y. **2020**. Nitric oxide and hydrogen peroxide increase glucose-6-phosphate dehydrogenase activities and expression upon drought stress in soybean roots. *Plant Cell Reports* **39**: 63–73.

Wang H, Yang L, Li Y, Hou J, Huang J, Liang W. **2016**. Involvement of ABA- and H_2O_2-dependent cytosolic glucose-6-phosphate dehydrogenase in maintaining redox homeostasis in soybean roots under drought stress. *Plant Physiology and Biochemistry* **107**: 126–136.

Wendt UK, Wenderoth I, Tegeler A, Von Schaewen A. **2000**. Molecular characterization of a novel glucose-6-phosphate dehydrogenase from potato (*Solanum tuberosum* L.). *The Plant Journal* **23**: 723–733.

Wieloch T. **2021**. A cytosolic oxidation–reduction cycle in plant leaves. *Journal of Experimental Botany* **72**: 4186–4189.

Wieloch T. **2022**. High atmospheric CO_2 concentration causes increased respiration by the oxidative pentose phosphate pathway in chloroplasts. *New Phytologist* **235**: 1310–1314.

Wieloch T, Augusti A, Schleucher J. **2022a**. Anaplerotic flux into the Calvin-Benson cycle. Hydrogen isotope evidence for *in vivo* occurrence in C_3 metabolism. *New Phytologist* **234**: 405–411.

Wieloch T, Augusti A, Schleucher J. **2023**. A model of photosynthetic CO_2 assimilation in C_3 leaves accounting for respiration and energy recycling by the plastidial oxidative pentose phosphate pathway. *New Phytologist* **239**: 518–532.

Wieloch T, Ehlers I, Yu J, Frank D, Grabner M, Gessler A, Schleucher J. **2018**. Intramolecular ^{13}C analysis of tree rings provides multiple plant ecophysiology signals covering decades. *Scientific Reports* **8**: 5048.

Wieloch T, Grabner M, Augusti A, Serk H, Ehlers I, Yu J, Schleucher J. **2022b**. Metabolism is a major driver of hydrogen isotope fractionation recorded in tree-ring glucose of *Pinus nigra*. *New Phytologist* **234**: 449–461.

Wieloch T, Sharkey TD, Werner RA, Schleucher J. **2022c**. Intramolecular carbon isotope signals reflect metabolite allocation in plants. *Journal of Experimental Botany* **73**: 2558–2575.

Wieloch T, Werner RA, Schleucher J. **2021**. Carbon flux around leaf-cytosolic glyceraldehyde-3-phosphate dehydrogenase introduces a ^{13}C signal in plant glucose. *Journal of Experimental Botany* **72**: 7136–7144.

Supporting information

Notes S1. Materials and Methods (expanded).

Notes S2. Hydro-carbon isotope fractionation during 1961 to 1980.

Notes S3. Estimated deuterium fractionation due to shifts of the phosphoglucose isomerase reaction.

Table S1. Shapiro-Wilk normality test.

Table S2. F and T test.

Table S3. Pearson correlations between Δ_i' and ε_{met} series of the period 1983 to 1995.

Table S4. Components of variance in Δ_i' series.

Table S5. Pearson correlation coefficients and associated levels of significance of ε_{met}-climate relationships for the period 1983 to 1995.

Table S6. Linear regression model of $\varepsilon_{met\ (H1)}$ as function of growing season air vapour pressure deficit (*VPD*) and March to July precipitation (*PRE*).

Figure S1. Air vapour pressure deficit of the growing season and March to July precipitation over the period 1961 to 1995 in the Vienna basin.

Table 1. Abbreviations and symbols.

Abbreviation	Definition
^{13}C signal	systematic $^{13}C/^{12}C$ variation
DAHPS	3-deoxy-D-arabino-heptulosonate 7-phosphate synthase
F6P	fructose 6-phosphate
G6P	glucose 6-phosphate
G6PD	glucose-6-phosphate dehydrogenase
GAP	glyceraldehyde 3-phosphate
GAPDH	glyceraldehyde-3-phosphate dehydrogenases
NMRS	nuclear magnetic resonance spectroscopy
OPPP	oxidative branch of the pentose phosphate pathway
PEP	phospho*enol*pyruvate
PEPC	phospho*enol*pyruvate carboxylase
PGA	3-phosphoglycerate
PGI	phosphoglucose isomerase
PK	pyruvate kinase
RuBP	ribulose 1,5-bisphosphate
TCAC	tricarboxylic acid cycle
Symbol	**Definition**
p_a	ambient CO_2 partial pressure
p_i	intercellular CO_2 partial pressure
PRE	precipitation
RAD	global radiation
SD	sunshine duration
$SPEI_i$	standardised precipitation-evapotranspiration index calculated for different timescales, i = 1, 3, 6, 8, 12, 16, 24, 36, 48 months
TMP	air temperature
VPD	air vapour pressure deficit
Δ	^{13}C discrimination denoting $^{13}C/^{12}C$ variation due to plant physiological processes
Δ_i'	intramolecular ^{13}C discrimination where i denotes individual glucose carbon positions and the prime denotes data corrected for ^{13}C signal redistribution by heterotrophic triose phosphate cycling
ε_{met}	metabolic deuterium fractionation at glucose H^1 and H^2

Table 2. Hydrogen isotope effects of phosphoglucose isomerase (PGI, Rose & O'Connell, 1961), and carbon isotope effects of glucose isomerase (GI, Gilbert *et al.*, 2012).

PGI, $\alpha = k_H/k_D$			GI, $\alpha = k_{12C}/k_{13C}$				
F6P, H^{1R}		**G6P, H^2**	**F6P, C-1**	**F6P, C-2**		**G6P, C-1**	**G6P, C-2**
	→	$2.\overline{2}$			→	1.005	1.015
<u>0.9</u>	↔	$\underline{1.\overline{1}}$	<u>1.013</u>	<u>0.993</u>	↔	0.987	1.007
2	←		<u>1.018</u>	<u>1.008</u>	←		

→ kinetic isotope effect, ↔ equilibrium isotope effect. Calculated values underlined. Since GI and PGI have the same reaction mechanism, the ^{13}C isotope effects of GI and PGI are thought to be very similar (Gilbert *et al.*, 2012). H^{1R}, *pro-R* hydrogen at F6P C-1.

Table 3. Significance of Pearson correlations among Δ_1', Δ_2', and Δ_3' and climate series for the period 1983 to 1995 (n = 13).

	VPD			*PRE*			*SPEI*$_1$			*SPEI*$_3$			*SPEI*$_4$			*SPEI*$_6$			*SPEI*$_8$			*SPEI*$_{12}$			*SPEI*$_{16}$			*SPEI*$_{24}$			*SPEI*$_{36}$			*SPEI*$_{48}$			*TMP*			*SD*			*RAD*		
Period / Δ_i'	**1**	**2**	**3**	**1**	**2**	**3**	**1**	**2**	**3**	**1**	**2**	**3**	**1**	**2**	**3**	**1**	**2**	**3**	**1**	**2**	**3**	**1**	**2**	**3**	**1**	**2**	**3**	**1**	**2**	**3**	**1**	**2**	**3**	**1**	**2**	**3**	**1**	**2**	**3**	**1**	**2**	**3**	**1**	**2**	**3**
MAMJ	c	a	b		a		b		a	b		a	a																								a					a			
MAMJJ	c		b	a	a	a	b		b	b		a	b		a	a			a																										
MAMJJA	c		b	b	a	a	c		b	c		b	b		a	b			a																		a								
MAMJJAS	c		b	b	b		b		a	c		b	c		a	b		a	b																							a			
MAMJJASO	c		b	a	a		b		a	c		a	c		a	b		a	b		a	a																			a			
MAMJJASON	c		b	a	a		b		a	b		a	c		a	b		a	b		a	a																	a		a			
AMJJ	c		c	a	a	a	a		b	b		b	b		b	b		a	a																				a						
AMJJA	c		c	a	a	a	b		b	c		b	c		b	b		a	b		a																a		a						
AMJJAS	c		b	a	b	a	b		b	c		b	c		b	b		a	b		a	a																			a			
AMJJASO	c		b	a	a		b		a	c		b	c		b	c		b	b		a	a		a															a		a			
AMJJASON	c		b	a	b		a		a	b		a	c		b	c		a	c		a	b		a																a		a			
MJJA	b		b	a			b		a	b		b	b		b	b		b	b		a	a		a													a		a			a			
MJJAS	b		b	b	a	a	b		a	c		b	c		b	c		b	b		a	b		a																a		a			
MJJASO	c		b	a			b		a	c		b	c		b	c		b	c		a	b		a																a		a			
MJJASON	c		b	a	a		a		a	b		a	c		b	c		b	c		a	b		a																a		a			
JJAS	b		b				a			b		b	b		b	c		b	b		a	b		a																					
JJASO	b		b							b		a	b		b	c		b	c		a	b		a																					
JJASON	b		a							b		a	b		a	b		b	c		b	b		a	a		a																		
JASO	a		a							b		a	b		a	c		b	c		b	b		a	a		a							a											
JASON	a		a							a			b		a	b		b	c		b	b		a	a		a							a											
ASON	c		a										a			b		a	c		b	b		a	a		a							a						b					

Significance levels: ≤ 0.05, a; ≤ 0.01, b; ≤ 0.001, c. Underscore denotes negative correlation. Climate parameters: *PRE*, precipitation; *RAD*, global radiation; *SD*, sunshine duration; *SPEI*$_i$, standardised precipitation-evapotranspiration index of different periods (i = 1, 3, 6, 8, 12, 16, 24, 36, 48 months); *TMP*, air temperature; *VPD*, air vapour pressure deficit. Climate data were averaged for all ≥ 4-month periods of the growing season (March to November). Months were abbreviated by their initial letters. Δ_1', Δ_2', and Δ_3' denote intramolecular ^{13}C discrimination at glucose C-1, C-2, and C-3, respectively. Glucose was extracted across an annually resolved tree-ring series of *Pinus nigra*.

Table 4. Linear regression models of Δ_1', Δ_2', Δ_3', and ε_{met} as function of ε_{met}, growing season air vapour pressure deficit (*VPD*) and March to July precipitation (*PRE*).

M1: Δ_1' ~ ε_{met} + *VPD*, 1983-1995			
R^2 = 0.87, $adjR^2$ = 0.84, p < 0.00004, n = 13			
	Estimate	**± SE**	***p* ≤**
Intercept	36.0	2.7	0.0000001
ε_{met}	-0.0187	0.0057	0.008
VPD	-0.0295	0.0047	0.0001
M2: Δ_2' ~ ε_{met} + *VPD*, 1983-1995			
R^2 = 0.62, $adjR^2$ = 0.54, p < 0.008, n = 13			
	Estimate	**± SE**	***p* ≤**
Intercept	17.6	4.5	0.003
ε_{met}	-0.0315	0.0097	0.009
VPD	-0.0111	0.0080	0.2
M3: Δ_3' ~ ε_{met} + *VPD*, 1983-1995			
R^2 = 0.64, $adjR^2$ = 0.57, p < 0.006, n = 13			
	Estimate	**± SE**	***p* ≤**
Intercept	14.5	2.1	0.00004
ε_{met}	-0.00615	0.00449	0.2
VPD	-0.0129	0.0037	0.006
M4: Δ_2' ~ ε_{met}, 1983-1995			
R^2 = 0.54, $adjR^2$ = 0.50, p < 0.004, n = 13			
	Estimate	**± SE**	***p* ≤**
Intercept	11.8	1.7	0.00002
ε_{met}	-0.0351	0.0097	0.004
M5: Δ_3' ~ *VPD*, 1983-1995			
R^2 = 0.57, $adjR^2$ = 0.53, p < 0.003, n = 13			
	Estimate	**± SE**	***p* ≤**
Intercept	14.3	2.2	0.000040
VPD	-0.0143	0.0037	0.0030
M6: Δ_1' ~ *PRE* + *VPD*, 1983-1995			
R^2 = 0.82, $adjR^2$ = 0.79, p < 0.0002, n = 13			
	Estimate	**± SE**	***p* ≤**
Intercept	27.8	4.4	0.00008
PRE	0.0146	0.0061	0.04
VPD	-0.0280	0.0058	0.0007
M7: Δ_2' ~ *PRE*, 1983-1995			
R^2 = 0.43, $adjR^2$ = 0.37, p < 0.02, n = 13			
	Estimate	**± SE**	***p* ≤**
Intercept	-1.84	2.79	0.52
PRE	0.0274	0.0096	0.016
M8: Δ_3' ~ *VPD*, 1961-1980			
R^2 = 0.13, $adjR^2$ = 0.07, p = 0.15, n = 18			
	Estimate	**± SE**	***p* ≤**
Intercept	12.3	3.8	0.006
VPD	-0.0112	0.0074	0.15
M9: Δ_1' ~ *PRE* + *VPD*, 1961-1980			
R^2 = 0.07, $adjR^2$ = 0, p > 0.55, n = 18			

	Estimate	± SE	$p \leq$
Intercept	18.6	4.8	0.0015
PRE	0.00273	0.00407	0.51
VPD	-0.00357	0.00781	0.65
M10: Δ_2' ~ *PRE*, 1961-1980			
R^2 = 0.05, $adjR^2$ = 0, p = 0.35, n = 18			
	Estimate	**± SE**	$p \leq$
Intercept	6.92	0.93	0.000002
PRE	0.00276	0.00286	0.35
M11: ε_{met} ~ *PRE* + *VPD*, 1983-1995			
R^2 = 0.71, $adjR^2$ = 0.66, p < 0.002, n = 13			
	Estimate	**± SE**	$p \leq$
Intercept	437	118	0.004
PRE	-0.777	0.164	0.0008
VPD	-0.082	0.155	0.61

ε_{met}, Δ_1', Δ_2', and Δ_3' denote hydrogen isotope fractionation caused by metabolic processes at glucose H^1 and H^2, and carbon isotope discrimination at glucose C-1, C-2, and C-3, respectively. Glucose was extracted across an annually resolved tree-ring series of *Pinus nigra* from the Vienna Basin.

Table 5. Significance of Pearson correlations among Δ_1', Δ_2', and Δ_3' and climate series for the period 1961 to 1980 (n = 18).

	VPD			*PRE*			*SPEI*$_1$			*SPEI*$_3$			*SPEI*$_4$			*SPEI*$_6$			*SPEI*$_8$			*SPEI*$_{12}$			*SPEI*$_{16}$			*SPEI*$_{24}$			*SPEI*$_{36}$			*SPEI*$_{48}$			*TMP*			*SD*			*RAD*		
Period / Δ_i'	**1**	**2**	**3**	**1**	**2**	**3**	**1**	**2**	**3**	**1**	**2**	**3**	**1**	**2**	**3**	**1**	**2**	**3**	**1**	**2**	**3**	**1**	**2**	**3**	**1**	**2**	**3**	**1**	**2**	**3**	**1**	**2**	**3**	**1**	**2**	**3**	**1**	**2**	**3**	**1**	**2**	**3**	**1**	**2**	**3**
MAMJ	a						a			a			a											a			a													a			a		
MAMJJ										a														a			a																	
MAMJJA																								a			a																	
MAMJJAS						a																		a			b			a														
MAMJJASO							a																	a			b			a														
MAMJJASON																								a			b			a														
AMJJ										a			a											a			b																	
AMJJA						a																		a			b																	
AMJJAS						b			a															a			b			a														
AMJJASO						a																		a			b			a														
AMJJASON						a																		a			b			a														
MJJA					a	a																		a			b			a														
MJJAS					a	b			a															a			b			a														
MJJASO						a																					b			a														
MJJASON						a																					b			a														
JJAS					a	b			a																		b			a			a											
JJASO																											b			a			a											
JJASON																											b			a			a											
JASO			a																								b			a			a											
JASON								a																			b			a			a											
ASON			a																								b			a			a											

Significance levels: ≤ 0.05, a; ≤ 0.01. Underscore denotes negative correlation. Climate parameters: *PRE*, precipitation; *RAD*, global radiation; *SD*, sunshine duration; *SPEI*$_i$, standardised precipitation-evapotranspiration index of different periods (i = 1, 3, 6, 8, 12, 16, 24, 36, 48 months); *TMP*, air temperature; *VPD*, air vapour pressure deficit. Climate data were averaged for all ≥ 4-month periods of the growing season (March to November). Months were abbreviated by their initial letters. Δ_1', Δ_2', and Δ_3' denote intramolecular ^{13}C discrimination at glucose C-1, C-2, and C-3, respectively. Glucose was extracted across an annually resolved tree-ring series of *Pinus nigra*.

Table 6. Significance of Pearson correlations among Δ_4', Δ_5', and Δ_6' and climate series for the period 1961 to 1995 (n = 31).

	VPD			*PRE*			*SPEI*$_1$			*SPEI*$_3$			*SPEI*$_4$			*SPEI*$_6$			*SPEI*$_8$			*SPEI*$_{12}$			*SPEI*$_{16}$			*SPEI*$_{24}$			*SPEI*$_{36}$			*SPEI*$_{48}$			*TMP*			*SD*			*RAD*		
Period / Δ_i'	**4**	**5**	**6**	**4**	**5**	**6**	**4**	**5**	**6**	**4**	**5**	**6**	**4**	**5**	**6**	**4**	**5**	**6**	**4**	**5**	**6**	**4**	**5**	**6**	**4**	**5**	**6**	**4**	**5**	**6**	**4**	**5**	**6**	**4**	**5**	**6**	**4**	**5**	**6**	**4**	**5**	**6**	**4**	**5**	**6**
MAMJ																						a			a																b			b	
MAMJJ		a			a			a			a														a															b			b	a
MAMJJA		a			a			a			a			a																										b			b	b
MAMJJAS		a									a			a			a																							b			b	b
MAMJJASO											a			a			a			a																				a			b	b
MAMJJASON		a												a			a			a																				a			b	b
AMJJ		b	a		b			c	a		b			a											a												a	a	a		c			c	a
AMJJA		b	a		b			b	a		b			b			a			a																		a	a		c	a		c	b
AMJJAS		a	a		a			b	a		b			b			a			a																			a		c	a		c	c
AMJJASO		a	a		a			b	a		a			b			b			a																			a		b			c	c
AMJJASON		a	a					a	a		a			a			a			a																			a		b			c	c
MJJA		b	a	a	a			b	a		c	a		b			b			a																		a	b		c	a		c	b
MJJAS		a	a	a	a			b	a		b	a		b	a		b			a																		a	b		b	a		b	c
MJJASO		a	a	a	a			b	a		b	a		b	a		b	a		a			a																a		b			b	c
MJJASON		a	a					a	a		a	a		b	a		b	a		b			a															a	b		a			b	c
JJAS		a	a								b	a		b	a		b			a			a																b			a		a	c
JJASO			a								b	a		b	a		b	a		a			a																a						c
JJASON		a	a								a	a		a	a		b	a		b			a																a					a	c
JASO			a								a	a		b	a		b	a		b			a										a												b
JASON			a									a		a	a		b	a		b	a		a																a						b
ASON					a												b	a		a			a																						b

Significance levels: ≤ 0.05, a; ≤ 0.01, b; ≤ 0.001, c. Underscore denotes negative correlation. Climate parameters: *PRE*, precipitation; *RAD*, global radiation; *SD*, sunshine duration; *SPEI*$_i$, standardised precipitation-evapotranspiration index of different periods (i = 1, 3, 6, 8, 12, 16, 24, 36, 48 months); *TMP*, air temperature; *VPD*, air vapour pressure deficit. Climate data were averaged for all ≥ 4-month periods of the growing season (March to November). Months were abbreviated by their initial letters. Δ_4', Δ_5', and Δ_6' denote intramolecular ^{13}C discrimination at glucose C-4, C-5, and C-6, respectively. Glucose was extracted across an annually resolved tree-ring series of *Pinus nigra*.

Table 7. Linear regression models of Δ_4', Δ_5', and Δ_6' as function of April to September global radiation (*RAD*), and March to October air temperature (*TMP*).

M1: $\Delta_{5\text{-}6}$' ~ *RAD* + *TMP*, 1964-1995			
R^2 = 0.72, $adjR^2$ = 0.70, p = 0.0000001, n = 28			
	Estimate	**± SE**	***p* ≤**
Intercept	26.0	3.1	0.00000001
RAD	-0.00843	0.00105	0.00000002
TMP	1.35	0.29	0.00009
M2: Δ_5' ~ *RAD* + *TMP*, 1964-1995			
R^2 = 0.66, $adjR^2$ = 0.64, p = 0.000001, n = 28			
	Estimate	**± SE**	***p* ≤**
Intercept	24.8	4.3	0.000005
RAD	-0.0103	0.0015	0.0000002
TMP	1.81	0.40	0.0001
M3: Δ_6' ~ *RAD* + *TMP*, 1964-1995			
R^2 = 0.47, $adjR^2$ = 0.43, p = 0.0003, n = 28			
	Estimate	**± SE**	***p* ≤**
Intercept	27.3	4.2	0.0000009
RAD	-0.00658	0.00144	0.0001
TMP	0.876	0.393	0.04
M4: $\Delta_{5\text{-}6}$' ~ *RAD* + *TMP*, 1964-1980			
R^2 = 0.69, $adjR^2$ = 0.63, p = 0.0009, n = 15			
	Estimate	**± SE**	***p* ≤**
Intercept	31.2	6.7	0.0006
RAD	-0.00906	0.00177	0.0003
TMP	1.11	0.47	0.04
M5: $\Delta_{5\text{-}6}$' ~ *RAD* + *TMP*, 1983-1995			
R^2 = 0.82, $adjR^2$ = 0.79, p < 0.0002, n = 13			
	Estimate	**± SE**	***p* ≤**
Intercept	29.1	4.5	0.00008
RAD	-0.00875	0.00132	0.00006
TMP	1.22	0.40	0.01
M6: Δ_4' ~ *RAD* + *TMP*, 1964-1995			
R^2 = 0.15, $adjR^2$ = 0.09, p = 0.12, n = 28			
	Estimate	**± SE**	***p* ≤**
Intercept	8.33	4.73	0.09
RAD	-0.00266	0.00160	0.11
TMP	0.931	0.439	0.04

Δ_4', Δ_5', and Δ_6' denote carbon isotope discrimination at glucose C-4, C-5, and C-6, respectively. Glucose was extracted across an annually resolved tree-ring series of *Pinus nigra* from the Vienna Basin.

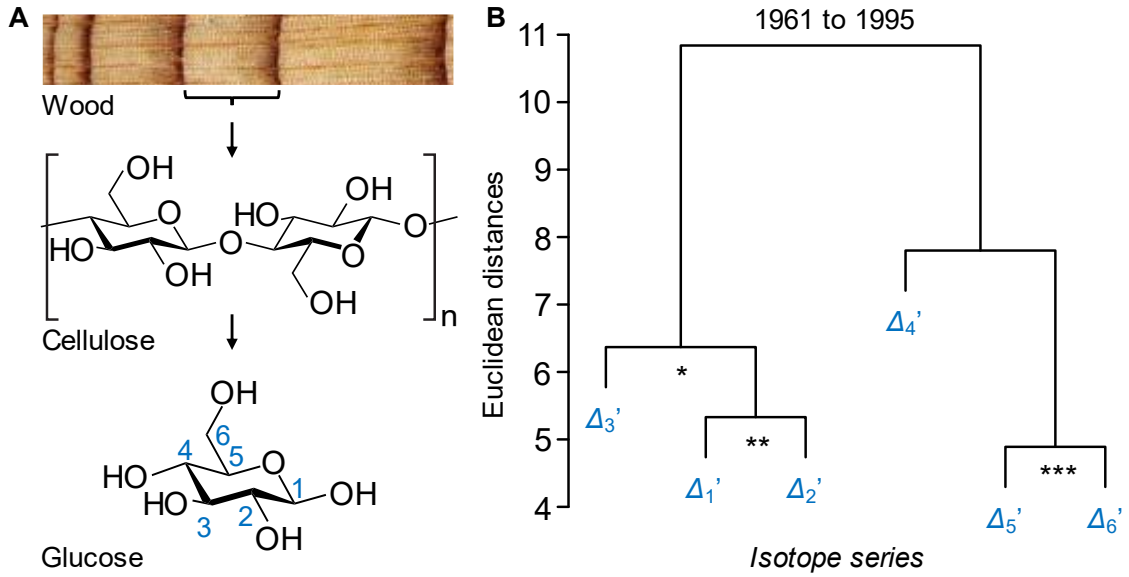

Figure 1. Carbon isotope discrimination in tree rings. (A) Levels of resolution of stable carbon isotope analysis: whole plant materials, whole molecules, intramolecular carbon positions. **(B)** Hierarchical clustering of Δ_i' series for the period 1961 to 1995. Significance of series correlation: *, $p \leq 0.05$; **, $p \leq 0.01$; ***, $p \leq 0.001$. Modified figure from Wieloch *et al.* (2018). Δ_i' denotes intramolecular ^{13}C discrimination in glucose extracted across an annually resolved *Pinus nigra* tree-ring series.

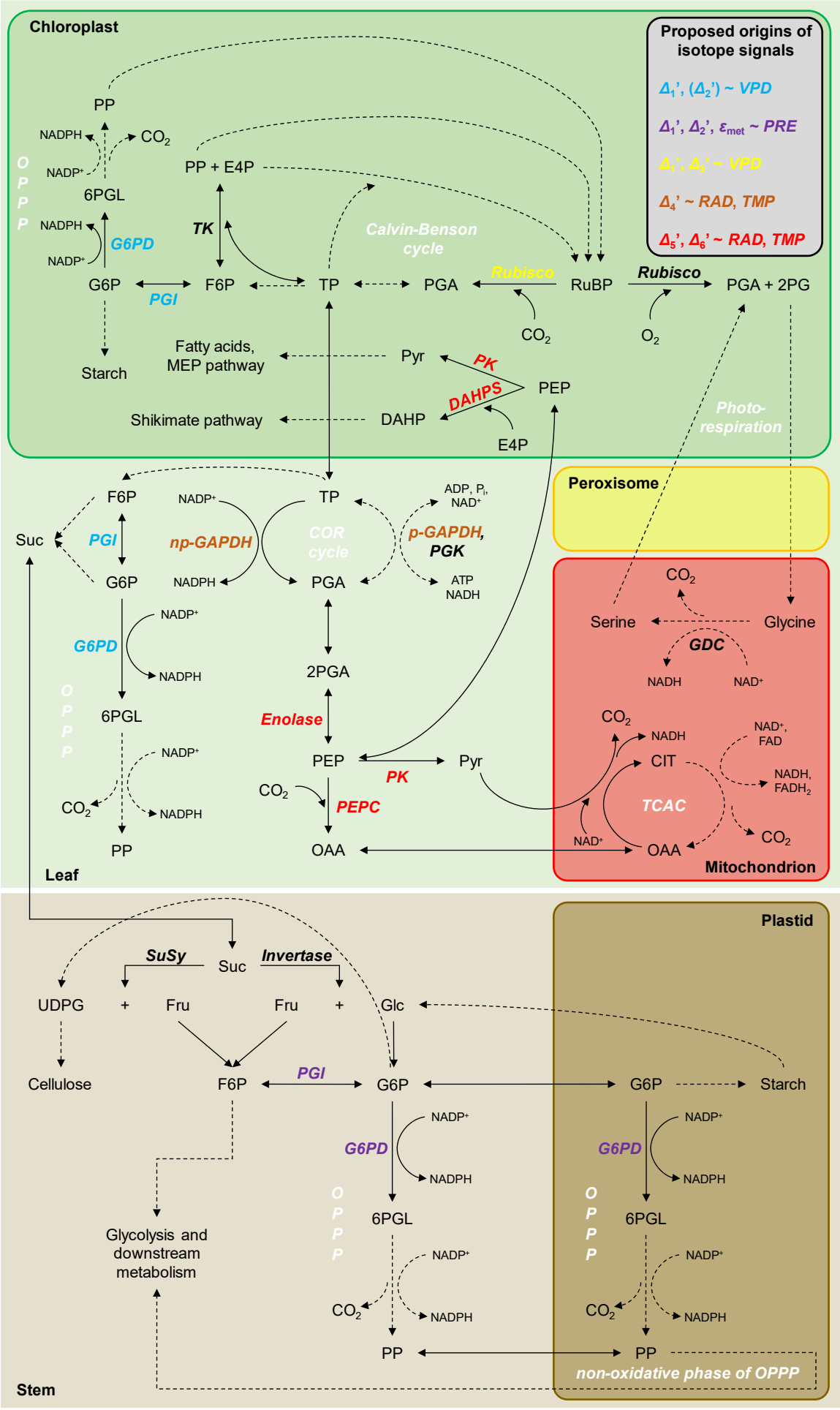
Chloroplast
Proposed origins of isotope signals
Δ1', (Δ2') ~ VPD
Δ1', Δ2', εmet ~ PRE
Δ1', Δ3' ~ VPD
Δ4' ~ RAD, TMP
Δ5', Δ6' ~ RAD, TMP
PP
NADPH
CO2
NADP+
OPPP
6PGL
PP + E4P
NADPH
NADP+
G6PD
TK
Calvin-Benson cycle
G6P
PGI
F6P
TP
PGA
Rubisco
RuBP
Rubisco
PGA + 2PG
CO2
O2
Starch
Fatty acids, MEP pathway
Pyr
PK
DAHPS
PEP
Shikimate pathway
DAHP
E4P
Photo-respiration
Peroxisome
F6P
NADP+
TP
ADP, Pi, NAD+
Suc
PGI
np-GAPDH
COR cycle
p-GAPDH, PGK
G6P
NADPH
PGA
ATP
NADH
CO2
Serine
Glycine
GDC
NADP+
NADH
NAD+
G6PD
NADPH
2PGA
OPPP
6PGL
Enolase
CO2
NADH
NAD+, FAD
NADP+
PEP
Pyr
CIT
NADH, FADH2
PK
CO2
NADPH
PEPC
TCAC
NAD+
CO2
PP
OAA
OAA
Leaf
Mitochondrion
Plastid
SuSy
Suc
Invertase
UDPG
+
Fru
Fru
+
Glc
Cellulose
F6P
PGI
G6P
G6P
Starch
NADP+
NADP+
G6PD
G6PD
NADPH
NADPH
OPPP
OPPP
6PGL
6PGL
Glycolysis and downstream metabolism
NADP+
NADP+
CO2
NADPH
CO2
NADPH
PP
PP
non-oxidative phase of OPPP
Stem

774

Figure 2. Proposed metabolic origins of carbon and hydrogen isotope signals in tree-ring glucose. Dashed arrows indicate that intermediate reactions are not shown. Abbreviations: 2PG, 2-phosphoglycolate; 2PGA, 2-phosphoglycerate; 6PGL, 6-phosphogluconolactone; ADP, adenosine diphosphate; ATP, adenosine triphosphate; CIT, citrate; COR cycle, cytosolic oxidation-reduction cycle; DAHP, 3-Deoxy-D-*arabino*-heptulosonate 7-phosphate; DAHPS, DAHP synthase; E4P, erythrose 4-phosphate; F6P, fructose 6-phosphate; FAD, flavin adenine dinucleotide; Fru, fructose; G6P, glucose 6-phosphate; G6PD, G6P dehydrogenase; GDC, glycine decarboxylase complex; Glc, glucose; MEP pathway, methylerythritol 4-phosphate pathway; NAD^+, nicotinamide adenine dinucleotide; $NADP^+$, nicotinamide adenine dinucleotide phosphate; np-GAPDH, non-phosphorylating glyceraldehyde-3-phosphate dehydrogenase; OAA, oxaloacetate; OPPP, oxidative pentose phosphate pathway; PEP, phospho*enol*pyruvate; PEPC, PEP carboxylase; p-GAPDH, phosphorylating glyceraldehyde-3-phosphate dehydrogenase; PGA, 3-phosphoglycerate; PGI, phosphoglucose isomerase; PGK, phosphoglycerate kinase; P_i, inorganic phosphate; PK, pyruvate kinase; PP, pentose phosphate; *PRE*, precipitation; Pyr, pyruvate; Rubisco, ribulose-1,5-bisphosphate carboxylase/oxygenase; RuBP, ribulose 1,5-bisphosphate; *RAD*, global radiation; Suc, sucrose; SuSy, sucrose synthase; TCAC, tricarboxylic acid cycle; TK, transketolase; *TMP*, air temperature; TP, triose phosphates (glyceraldehyde 3-phosphate, dihydroxyacetone phosphate); UDPG, uridine diphosphate glucose; *VPD*, air vapour pressure deficit; Δ_i', intramolecular ^{13}C discrimination where *i* denotes individual glucose carbon positions and the prime denotes data corrected for ^{13}C signal redistribution by heterotrophic triose phosphate cycling; ε_{met}, metabolic deuterium fractionation at glucose H^1 and H^2.

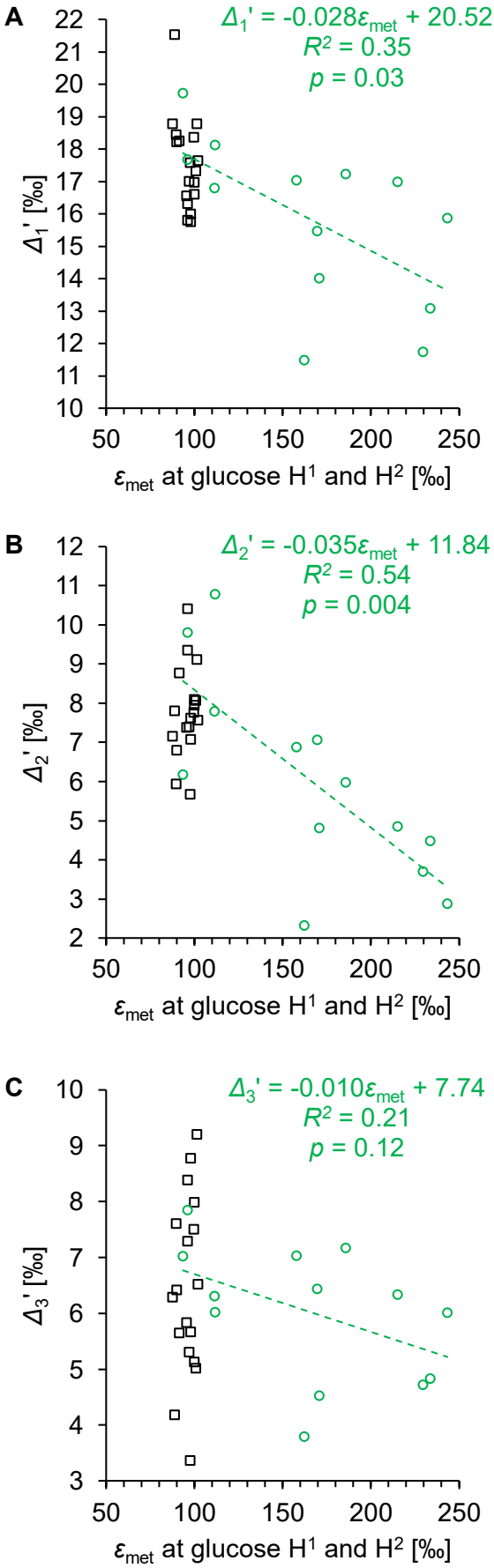

Figure 3. Relationship between the average hydrogen isotope fractionation caused by metabolic processes at glucose H^1 and H^2 (ε_{met}) and ^{13}C discrimination at C-1, C-2, and C-3 (Δ_1', Δ_2', and Δ_3'). Glucose was extracted across an annually resolved tree-ring series of *Pinus*

nigra from the Vienna Basin (black squares, 1961 to 1980; green circles, 1983 to 1995). Dashed line, relationship between the hydrogen and carbon isotope data of the period 1983 to 1995.

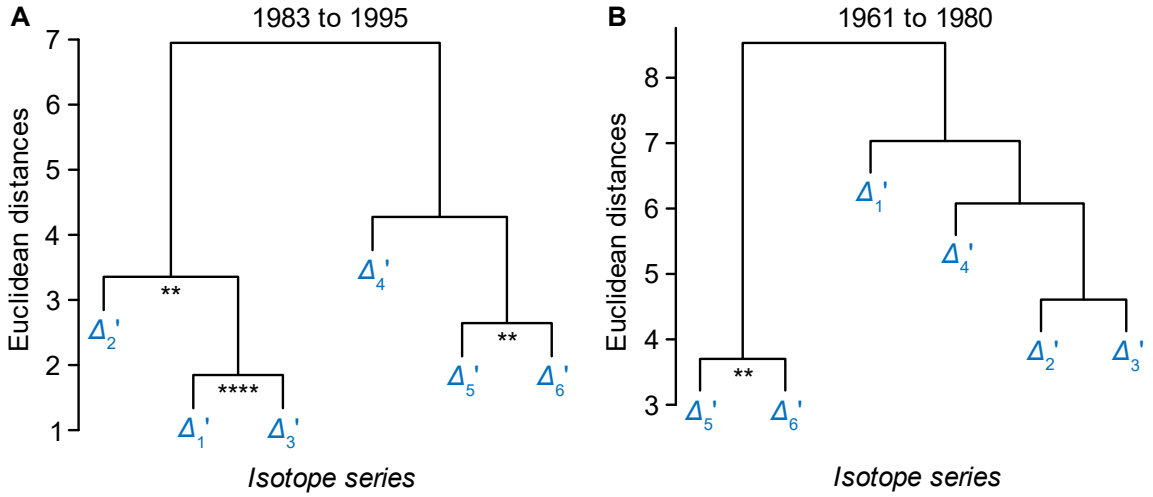

Figure 4. Hierarchical clustering of Δ_i' series for the periods 1983 to 1995 (A) and 1961 to 1980 (B). Δ_i' denotes intramolecular ^{13}C discrimination in tree-ring glucose of *Pinus nigra* from the Vienna basin with *i* denoting individual glucose carbon positions. Significance of series correlation: **, $p \leq 0.01$; ****, $p \leq 0.0001$.

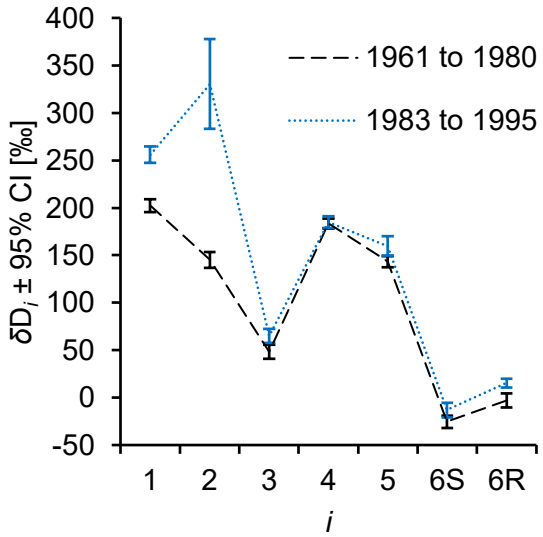

Figure 5. Average intramolecular δD_i patterns of the periods 1961 to 1980 and 1983 to 1995 (black and blue, respectively). The data were acquired for tree-ring glucose of *Pinus nigra* laid down at a site in the Vienna basin. The figure shows discrete data. Dashed and dotted lines were added to guide the eye. Data reference: Average deuterium abundance of the methyl-group hydrogens of the glucose derivative used for NMRS measurements. Modified figure from Wieloch *et al.* (2022b).